OPTICAL ANALYSIS OF MICROSCOPE IMAGES

Jonathan R. Biles
B.A. Physics, Reed College, 1977
M.A.Teaching Reed College, 1980

A dissertation submitted to the faculty
of the Oregon Graduate Center
in partial fulfillment of the
requirements for the degree
Doctor of Philosophy
in
Applied Physics
October, 1986

The dissertation "Optical Analysis of Microscope Images" by Jonathan Biles has been examined and approved by the following Examination Committee:

F. Paul Carlson, Thesis Advisor
Professor of Applied Physics and Electrical Engineering
President of the Oregon Graduate Center

Charles Miles
Professor Emeritus of Pathology,
University of Utah Medical School

J. Fred Holmes
Chairman of Applied Physics and Electrical Engineering

Rao Gudimetla
Assistant Research Professor of Applied Physics and Electrical Engineering

Richard Kieburtz
Chairman of Computer Science and Engineering

Acknowledgements

The greatest thanks goes to Drs. F.P. Carlson and Charles Miles for helping advise this thesis, and to the Cal Souther Foundation for supporting it. Drs. F. Holmes, R. DeFreez, R. Gudimetla, and R. Elliott all helped with my general graduate education in optics. A great deal of lab space and equipment, such as Dr. Holmes' Argon laser, Dr. Elliott's frame grabber, and Dr. DeFreez's video camera were lent to me by members of OGC. Dr. A. Rashad of OHSU (Oregon Health Sciences University) also helped me by supplying color slides of bacteria. Dr. Paolo Dobrillo helped print out the frame subtractor's images.

Table of Contents

List of Figures

ABSTRACT

Optical Analysis of Microscope Images

Jonathan Biles, Ph.D.
Oregon Graduate Center, 1986

Supervising Professor: F. Paul Carlson

Microscope images were analyzed with coherent and incoherent light using analog optical techniques. These techniques were found to be useful for analyzing large numbers of nonsymbolic, statistical microscope images.

In the first part phase coherent transparencies having 20-100 human multiple myeloma nuclei were simultaneously photographed at 100 power magnification using high resolution holographic film developed to high contrast. An optical transform was obtained by focussing the laser onto each nuclear image and allowing the diffracted light to propagate onto a one dimensional photosensor array.

This method reduced the data to the position of the first two intensity minima and the intensity of successive maxima. These values were utilized to estimate the four most important cancer detection clues of nuclear size, shape, darkness, and chromatin texture.

In the second part, the geometric and holographic methods of phase incoherent optical processing were investigated for pattern recognition of real-time, diffuse microscope images. The theory and implementation of these processors was

discussed in view of their mutual problems of dimness, image bias, and detector resolution.

The dimness problem was solved by either using a holographic correlator or a speckle free laser microscope. The latter was built using a spinning tilted mirror which caused the speckle to change so quickly that it averaged out during the exposure.

To solve the bias problem low image bias templates were generated by four techniques: microphotography of samples, creation of typical shapes by computer graphics editor, transmission holography of photoplates of samples, and by spatially coherent color image bias removal. The first of these templates was used to perform correlations with bacteria images. The aperture bias was successfully removed from the correlation with a video frame subtractor.

To overcome the limited detector resolution it is necessary to discover some analog nonlinear intensity peak detector which would allow one sampling point to determine if the correlation intensity was high anywhere in the correlation output.

Three specific medical uses for the intensity correlators are detailed.

INTRODUCTION

Optical Information Processing (OIP) usually involves a linear transformation of the input object to an output image. Every imaging system does such a transformation. The linear system theory used to describe an imaging process is the basis of most first-order physics and engineering analysis methods, and is described by the generic equation:

$$Out(\Delta x) = \int In(x) Resp(x + \Delta x) dx$$

The impulse response (Resp) is the system's response to a delta (δ) function "spike". Δx is the translation of the *Response* relative to the *Input*. The impulse response fully characterizes the transforming system.

OIP has three definitive useful characteristics:

1) Effective large memory due to molecular level storage.

2) Simultaneous (or parallel) processing at the speed of light.

3) Associative processing by correlation.

These abilities make OIP an ideal candidate for use in carrying out the many rapid correlations required of pattern recognition. Our three-dimensional (3-D) continuous real world is much vaster than just the countable integers, so it is not surprising that it is difficult to reduce the real world to a finite string of computer symbols. Going from an image of a real tree to the machine knowledge that there is a tree in the image is always done by correlating the input image with images of other trees, or with abstract shapes which can be combined to represent trees. It

must be done with analog data to "symbolize" it. There will be no study here of the validity of correlation for pattern recognition, the goal (of the second chapter) is to achieve it by optical methods. Also, throughout this thesis the term "correlation" may be used where "convolution" would be more appropriate, since these two operations differ only by an inversion of one of the functions.

If the impulse response in the above equation is the image to be recognized, then the output will be the correlation of the input with the impulse response. The x and y coordinates of the output will be the values of the separations of the two correlated functions $(\Delta x,\Delta y)$. Intuitively, this means to lay them over each other and see if they line up in the sense of having their values rise and fall together. This simple measure of similarity is naturally sensitive to rotation and scaling changes in the input. Even this simple correlation is a long calculation for a digital computer, because the value at each correlation point $(\Delta x,\Delta y)$ is made of many pointwise multiplications which are all summed, then shifted, multiplied again, summed again, and so on for every point in the correlation.

Crystallographers were the first to use geometrically based OIP systems to correlate crystal structures. [1] The input image was looked at through a transparent image of a known crystal structure to be recognized (called a template) and moved around until the template lined up with the input, at which point the crystal was recognized. With the invention of the laser, spectacular results were achieved in coherent OIP with transparencies, yet most scientists became very disillusioned when no inexpensive alternative was found to having to use a transparency as an input. Computers were becoming so successful at information processing in general that OIP with transparencies seemed a wasted research effort,

although a few researchers did continue trying to use non-transparent (incoherent) images as input. This thesis traces that path into new uses in microscope image pattern recognition.

There is a great need for optical analysis of microscope images. The need to evaluate microscope samples is worldwide. Microscopic analysis is essential in hospitals and in many industrial situations such as water sanitation control. But, the high numerical aperture objectives necessary in these applications have small areas of view. [2] Thus to examine a single slide many images need to be analyzed. In order for image analysis to be applied to flowing cell analyzers, 5000 cells/second would need to be examined. [3] It would be very helpful if all these images could be screened by analog optical correlations so that a human or computer need only study the most important ones. This thesis identifies simple methods of accomplishing this prescreening process.

The outline of this thesis follows a chronological sequence. Two chapters show a transition from the old coherent methods of Chapter 1 to the incoherent processes of Chapter 2. The first chapter describes the early coherent pattern recognition work done with Dr. Charles Miles on image analysis of photographs of nuclei. The major problem encountered was the need for a photograph of the nuclei, so it was decided to pursue further work analyzing the original incoherent microscope image rather than a transparency.

The second chapter deals with this incoherent image analysis. It has two means of implementation: holographic and geometrical. The holographic method is based totally on diffraction, so its resolution is very good when using monochromatic light. The geometrical method assumes that diffraction has no effect, so

image detail is limited, but white light and colored slides may be used. These holographic and geometrical methods were experimentally examined and compared. The results show promise for incoherent OIP, especially if an analog nonlinear method of peak detection is discovered.

Chapter I

SIZE, SHAPE, DARKNESS, AND TEXTURE OF HUMAN CELL NUCLEI DERIVED FROM THE DIFFRACTION PATTERN OF THEIR PHOTOGRAPHS

Abstract

Phase coherent transparencies having 20-100 human multiple myeloma nuclei are simultaneously photographed at 100 power magnification using high resolution holographic film developed to a high contrast gamma. An optical transform of the nuclear images was obtained by focussing the laser onto each nuclear image and allowing the diffracted light to propagate onto a one dimensional 1024 element charge coupled device (CCD) array.

This method reduced the total data to a few values of the position of the first two intensity minima and the intensity of successive maxima. These measurements could be readily obtained from the data by null slope detectors. These measurements were then utilized to create estimates of the four most important cancer detection clues of nuclear size, shape, darkness, and chromatin texture. The calculations were simple, but a transparent image was required as input.

1.2) Introduction

By use of a Fourier transform any naturally generated waveform can be represented as a sum of its frequency domain components. In particular, an image of a cell nucleus can be represented by a sum of grating-like spatial frequencies of various amplitudes. While it is obvious that a frequency representation simplifies periodic structures, frequency representations can also be shown to simplify stationary random data of large dimensionality [4]. Nuclear images, and especially their texture, appear to be good candidates for spatial frequency domain analysis due to the statistical nature of the many contributing variables.

The far-field optical diffraction pattern of an aperture is the frequency domain representation (Fourier transform) of the aperture [5]. Since this frequency representation is obtained at the speed of light by diffraction, it may be very useful for flowing cell analyzers which must examine thousands of nuclei each second.

Successful work has been done on spatial frequency representations of nuclear images, the most complete work being done by Pernicke and colleagues [6]. The major problems were 1) that the cytoplasm's higher index of refraction acted like a small lens to defocus the undiffracted light which then distorted the nuclear diffraction pattern and made the information about the nucleus difficult to detect, and 2) that the original dark nucleus on a clear background allowed the unblocked portion of the focussed laser's gaussian intensity pattern to pass around the nucleus, convolving a gaussian intensity (the far field diffraction of the original gaussian) onto the nucleus' diffracted signal. One group of researchers managed to extract nuclear size information from optical transforms of the actual nucleus, but

with great difficulty because of the above two problems. [7]. Pernicke used an expensive liquid crystal light valve [8] to "photograph" the nuclei in real-time. The poor performance of this light valve was the weakest part of the process, and they concluded their paper with a suggestion that: "Mention should be made of the possibility of using high quality photographic copies of a complete smear rather than photographing individual cells alone ... The contrast ratio available with film makes the use of photography for the input medium an attractive feature." Implementation of such a device which photographs an entire field of cells is the first contribution of this chapter.

The other contribution is the immediate reduction of transform data by simple data sorting and calculation to form estimates of the four parameters of size, shape, darkness, and texture which pathologists have learned can be used to discriminate cancerous nuclei.

Figure 1.1 First optical transform setup.

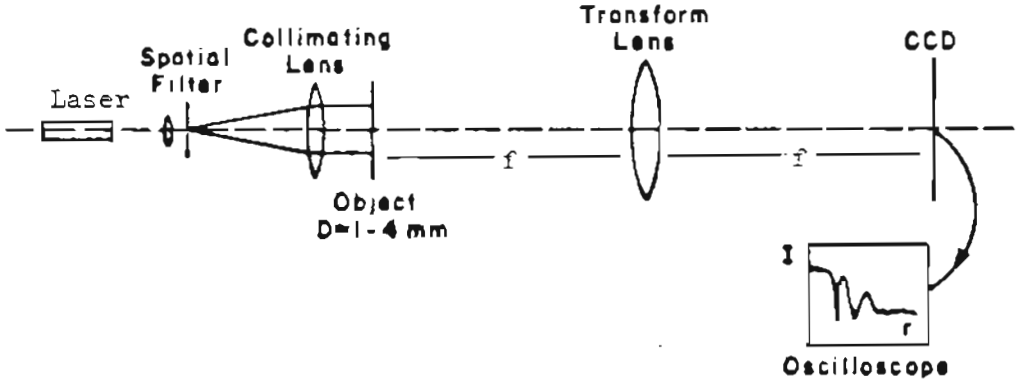

Figure 1.2 Microscope setup for making photoplates.

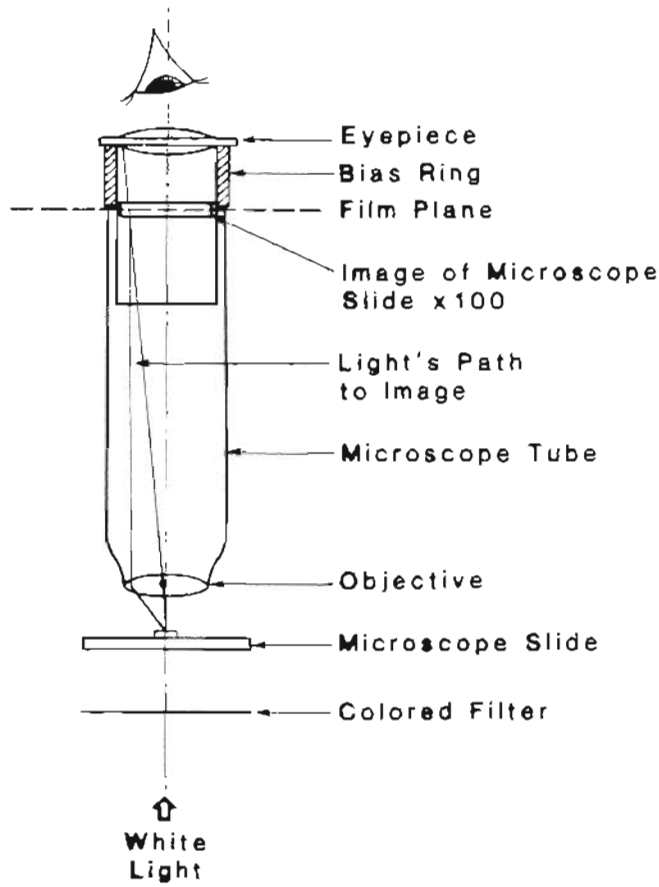

Figure 1.3 The exposure increases from left to right on these 1X negatives of four photoplate exposures. The circular outline is from the microscope tube. In the longest exposure only the purple nuclei have not sent enough light through the green filter to expose the film.

Figure 1.4 A 20X negative enlargement of a photoplate showing many nuclei.

Figure 1.5 Improved optical transform setup.

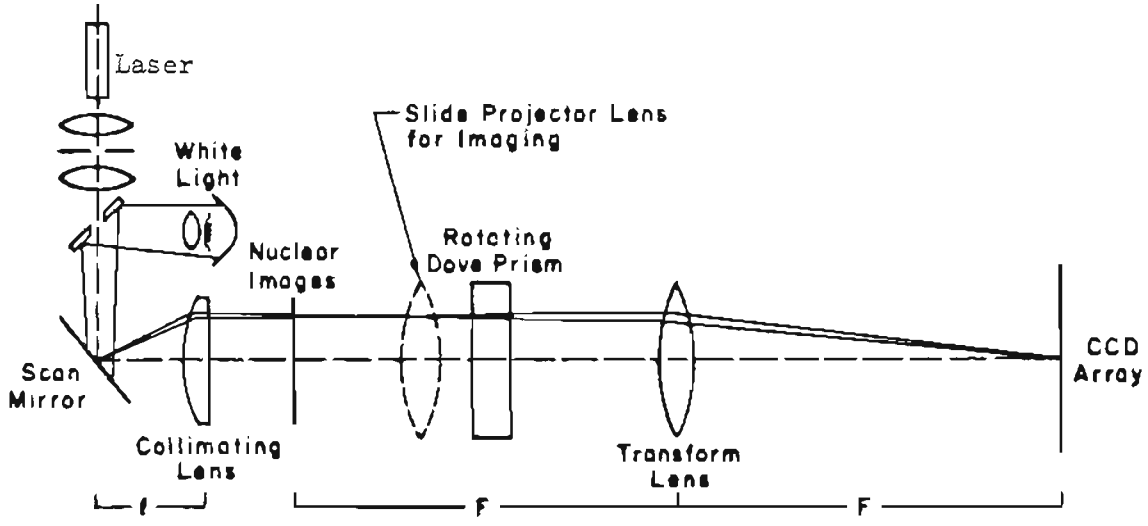

1.3) Materials and Methods

The apparatus used for initial measurement was similar to that previously described, [9] except that the nuclear diffraction patterns were projected onto a one dimensional charge coupled device (CCD) array as illustrated in figure 1.1 . Light from a Helium Neon laser was spatially filtered, collimated, and sent through a transparent object consisting of 1-4mm nuclear images. The diffraction pattern of each nucleus was cast by the transform onto the CCD array.

High contrast photomicrographs of single nuclei on 35mm film supplied by Dr. Miles were used initially. Later on in the research, a special photomicrographic technique was developed to photograph an entire field of nuclei.

1.31) Photomicrograph of Multiple Nuclei

In order to get the microscope's intermediate real image to lie in a plane at the top of the microscope tube, the eyepiece was raised slightly by a "bias ring". When the virtual image of a cell was seen clearly by an eye which is relaxed to focus at infinity, the eyepiece could be removed, Kodak 131 holographic plates could be placed emulsion side down on top of the microscope tube, and exposed to the focussed real image. The microscope illuminator was filtered into a complementary color strongly absorbed by the nuclear stain (usually green light for a purple hematoxylin stain) See figure 1.2 . These photoplates were then developed in Kodak D8 high contrast developer [10] which makes the image of the unstained cytoplasm completely opaque. Since the images have been magnified 100 times by

the single oil immersion lens, the result is that 20-100 cells in the large field are all accurately recorded with the 2000 line/mm resolution of the holographic film. This ensures that the limiting resolution is that possible with the oil immersion lens. This resolution theoretically is:

$$r = \frac{1.22\lambda}{2(numerical\ aperture)}$$

This resolution equals .251 micron for .514 micron green light going through an oil immersion objective with a numerical aperture of 1.25. A barely resolved feature when magnified 100 times is 25 microns, fifty times larger than the half micron resolution of the holographic film. See figures 1.3 and 1.4 for examples of these photoplates.

1.32) Optical transform setup

On the microscope image plate each of the many nuclear images is a little less than .5 mm. In order to get sufficient light through only a nucleus the laser must be focussed onto that nucleus. The focus of the laser beam is called its waist, and at this point the light waves are planes perpendicular to the light's direction of travel. This beam waist diameter w is approximately equal to the F number of the lens times the wavelength of the light. [11] To achieve this beam waist, the laser is spatially filtered through a pinhole and then focussed onto the pivoting point of a scanning mirror which is the focal point of a collimating lens. See figure 1.5 . Since all light coming from the focal point of a lens is collimated by the lens parallel to the optical axis, this collimated beam can be shifted to illuminate any individual

nucleus of the image plate by tilting the mirror. The translation invariance of the Fourier transform ensures that all these shifted but parallel beams produce transforms centered about the optical axis. The transforms are measured by a one inch, 1024 linear element CCD array which drives the input to an oscilloscope.

A slide projector lens images the 1 inch diameter photoplate onto the CCD array, allowing a nucleus to be measured directly as an object. A background field of white light is added by a mirror with a hole for the laser, so the entire field of many nuclei is projected onto a screen around the CCD array. This allows one to examine a large area at once with speckle free white light, choose one nucleus, and move the laser over to measure its diffraction pattern.

The diffraction pattern of an object which has a uniform index of refraction is always symmetric about the origin. [12] Since the photographs of the nuclei are in an index matching liquid gate [13] there is no phase variation, and only one half of the transform needs to be examined. The oscilloscope traces of the intensity across 6 radii of a semi-circle of the transform were photographed. This was done by rotating the image 30 degrees between each radius measurement and keeping the CCD array fixed in the horizontal position. Six different nuclear diffraction patterns were examined in detail and they are shown, along with their nuclei, in the upper right of figures 1.9 - 1.14. Each of these nuclei has six oscillograms of its radii at 30 degree spokes shown to the left on the same page.

The many small nuclear images on a photoplate cannot easily be rotated about the optical axis, so a rotatable dove prism was used to rotate the image and the transform. Alignment and use of such prisms requires care. [14] Dove prisms are the same optically as refraction of light through a tilted plate of glass as thick

as the prism is long. Such tilted plates produce astigmatism in non-collimated wavefronts which decreases with increasing radius of curvature of the wavefront. The dove prism was therefore placed after the slide projector lens because the distant image from this lens develops little astigmatism when its nearly parallel rays pass through the dove prism, and the residual was corrected with a cylindrical eyeglass lens.

1.41) Detection Theory

A physical pattern may be represented in the object domain by a photograph of its image or in the frequency domain by the far field diffraction pattern of that photograph. A point which is a 2-dimensional vector $\vec{k}=k\hat{k}$ from the center of this diffraction pattern corresponds to an infinite plane wave grating in the original image with wave vector $\hat{k}(1/k)$. Presence of diffracted light at this point $\vec{k}$ indicates scattering edges in the photograph corresponding to a grating of period (1/k) but with any shifted phase, since we are detecting the intensity and not the phase of the diffracted light.

Our nucleus tends to have more circular symmetry than rectangular, so a polar (r,Θ) coordinate system works better than a cartesian (x,y) one. The corresponding basic Fourier transform will then be a Bessel function and not a $\frac{\sin(x)}{x}$ pattern.

The intensity of the diffracted light from a round hole theoretically falls off

with radius as:

$$I(r)=\left[\frac{kd^2}{8z}\right]^2\left\{\frac{2J_1\left[\frac{kdr}{2z}\right]}{\frac{kdr}{2z}}\right\}^2$$

where:

J_1 = the first order Bessel function

k= 2π/ wavelength of the light

d= the diameter of the diffracting hole

z= the distance to the screen

Table 1.1 Values for the minima and maxima where $x = \frac{(kd)}{(2z)}\, r$.

x	$\frac{2J_1(\pi x)}{\pi x}$	^{2} max or min
0	1.0	center
1.220	.0	min
1.635	.0175	max1
2.233	.0	min1
2.679	.00416	max2
3.238	.0	min2
3.699	.0016	max3
4.710	.00078	max4
5.715	.000436	max5
6.718	.000303	max6

Only the first few values of table 1.1 could be found from the literature, [15] so the last ones were calculated directly from a power series expansion of the first order Bessel function with a hand calculator. Using values from the above table, we expect the diffraction rings to fall off with the following ratios:

max2/max1 = .00416 / .01750 =.24

max3/max2 = .00160 / .00416 = .38

max4/max3 = .00078 / .00160 = .49

max5/max4 = .000436 / .00078 = .56

max6/max5 = .000303 / .000436 = .70

Figure 1.6 Form of oscilloscope display from which all data is taken. It is the intensity along one radius of the diffraction pattern of a circular aperture.

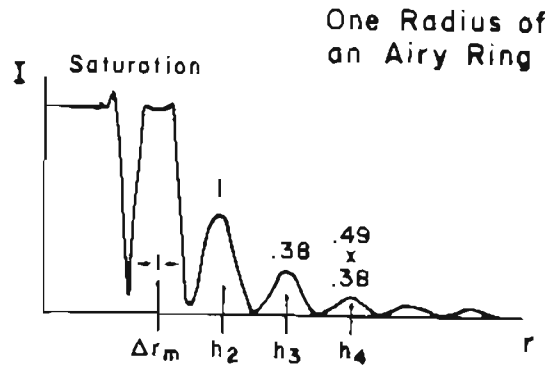

As can be seen from figure 1.6, in our experiments we saturated our CCD detector with both the central peak and the first ring, since these 2 are much larger than the later rings. Our experimentally derived ratio for the intensity of the diffraction maxima from a photograph of a perfectly clear round circle was in very good agreement with the above theoretical values except for the second ratio (the first one we measured) which was experimentally measured to be .33 instead of .38. This and the other closer ratios were only achieved if 1) the very intense-on axis undiffracted light was blocked before striking the CCD array, and 2) the incident light was really a uniform intensity plane wave. One of these errors could still account for the low value of the second ratio.

1.42) Data Analysis

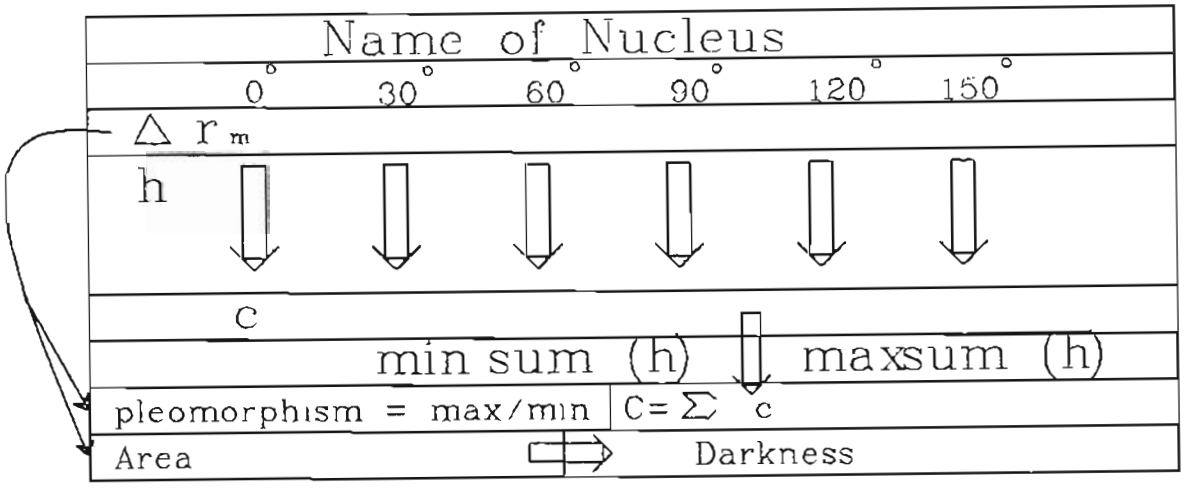

Figure 1.7 Data format

The data for each of the six nuclei is presented in figures 1.9 through 1.14 in the above tabular form. The second row of the tables show the angles of the six radial spokes of data from the nuclear images. The distances between the first two minima for each radial spoke (Δr_m) are shown in the third row. These will be used to calculate both the pleomorphism and the area. The area will be used, along with the light intensity at the origin, to calculate the average darkness of each nucleus. Each diffraction ring's height values (h) will be analyzed to give a chromatin value for each column of data of one angular spoke measurement. The individual values will then be added to give the nucleus' chromatin value C.

1.421) Nuclear Diameter

The distance between the first two minima of the transform of a circle of diameter D is:

$$\Delta r_m = r_{m2} - r_{m1} = 2.233\lambda\frac{z}{D} - 1.22\lambda\frac{z}{D} \approx \lambda\frac{z}{D} = \frac{const.}{D} .$$

The constant was found from the diffraction pattern of a calibrated hole. Since our nuclei are not perfect circles, we can only derive an approximate average diameter. This diameter is the average separation of all edges perpendicular to the CCD angle. Six approximate diameters of the diffracting nucleus (every 30 degrees) were found from the 6 $\Delta r_1,\ldots,\Delta r_6$ of its diffraction pattern. This can be seen by comparing the large size of all the Δr_m for the elliptical and hexagonal nuclei with the small size of all the Δr_m for the two big triangular and oval nuclei. A quantitative performance check was that the length to width ratio of the rectangular nucleus =4.5/2.5 is close to the ratio of the largest null separation to the smallest null separation of its diffraction pattern.= 16.6/8.4. The rest of the nuclei also compared favorably with hand estimates of the average diameter of the magnified nuclear images.

Figure 1.8 Nuclear area approximated by six triangles.

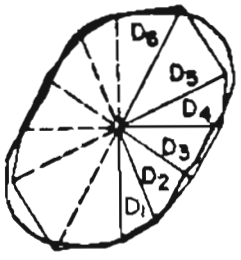

$$\text{Area} = \text{Const} \cdot \frac{\sum_{i=1}^{6} D_i^2}{\sum_{i=1}^{6} \frac{1}{\Delta r_{mi}^2}}$$

1.422) Nuclear Area

The six radial diameters found above defined a polygon made of 12 triangles (one every 30 degrees), whose opposites inverted about the center were identical (because of the inversion symmetry of real valued object transforms). See Fig. 1.8 . The separation of the first two nulls was measured, squared, and summed for all 6 radii. This number was multiplied by 100 for easier representation. Magnified nuclear images measured by hand on graph paper again indicated good predictions. These measured areas, shown above their predicted areas are: small hexagonal nucleus = 20.5/4.4 = 4.6, small rectangular nucleus = 22.5/6.1=3.7, small triangular nucleus = 21.5/5.9 = 3.6, large oval nucleus = 45/13=3.5, large triangular nucleus with coarse chromatin = 53/8.6=6.2. All these ratios are within 15 percent of 4.0 except the large triangle with very coarse chromatin. This nucleus is much larger than the separation of the nulls of its diffraction pattern suggests. If the internal opaque chromatin is neglected in measuring the area of the nucleus, then the ratio changes to 43/8.6=5, only 25 percent off of 4.0. One explanation of

this deviation begins by noticing that in this nucleus the chromatin appears as clumps attached to the side of the nuclear membrane. These effectively shorten the estimated diameters, which lessen the estimated area.

1.423) Darkness (Hyperchromasia)

Hyperchromasia is here defined as one over the average transmittance of a nucleus. This will now be shown to be approximately the ratio of the square of the nuclear size to the amount of on-axis light transmitted. This can be shown by starting with the definition of the average value of a function :

$$<f>=\frac{\int\int_{-\infty}^{\infty} f(x,y)\,dx\,dy}{\int\int_{-\infty}^{\infty} dx\,dy}$$

This integral can be related to the value of the transform of the amplitude transmittance $(+\sqrt{t})$ evaluated at the origin $=\sqrt{\textit{Intensity on the optical axis}}$. Beginning with the Fourier transform generating an intensity power spectrum.

$$I(u,v) = \left\{\int\int_{-\infty}^{\infty}\sqrt{t(x,y)}e^{-i2\pi(xu+yv)}dx\,dy\right\}^2$$

Substituting u=0, v=0 for on the optical axis.

$$I(0,0) = \left\{\int\int_{-\infty}^{\infty}\sqrt{t(x,y)}dx\ dy\right\}^2$$

The term in the brackets is equal to the above definition of average value for $f = \sqrt{t}$ multiplied by the area of the aperture.

$$= \left\{ <\sqrt{t}>\int\int_{-\infty}^{\infty} dx\,dy\right\}^2$$

$$= \left\{<\sqrt{t}>(\textit{area of aperture})\right\}^2$$

Since both terms are positive:

$$= <\sqrt{t}>^2(\textit{area of aperture})^2$$

Using the well known identity for the variance, $\sigma^2=<x^2>-<x>^2$ and substituting in $\sqrt{t}$ for x gives $\sigma^2=<t>-<\sqrt{t}>^2$. Assuming the variance is small, we can try approximating $<\sqrt{t}>^2$ *with* $<t>$.

$$I(0,0) = \langle t \rangle (area\ of\ aperture)^2$$

$$Hyperchromasia\,\% \equiv \frac{1}{\langle t \rangle} = \frac{area\ of\ nucleus^2}{I(0,0)}$$

The area of the aperture contributes proportionately once for the total energy transmitted and again due to its creating a lower F number which concentrates the energy into a smaller spot around I(0,0) . I(0,0) was measured by a photodiode on the optical axis. It's value for a calibrated hole was used to normalize I(0,0) for other nuclei. The assumption of small variance will be good for the nuclei 1.9-1.12 which have no chromatin clumping. For the last two nuclei, which have clumped chromatin, the assumption is less valid.

The photodiode doesn't really measure I(0,0). It, having a finite area, measures $\int_{one\ edge}^{other\ edge} I(x,y)\,da$. This study used a less than $1 mm^2$ photodetector, but it may have integrated in some of the low spatial frequencies.

1.424) Chromatin Texture

As lumps of chromatin appear in the image of the nucleus, they create high spatial frequencies which cause light to diffract out to the periphery of the transform in an irregular way. A measure of this irregularity is the variation from the expected fall off of the Airy ring peaks. The inner diffraction pattern, produced by the low frequency of the nucleus' shape and size, is isolated from the higher spatial frequencies of the chromatin texture.

Our measure of chromatin clumping, C, is the mean square variation from the theoretical decay of the Airy ring peaks for a clear circle.

To calculate C for each array reading, the heights of the first 5 experimental diffraction peaks were measured. Values under 1.0 mm were ignored because of the inaccuracy of measuring them by hand with a ruler. The square of the differences of experimental diffraction ring height ratios from the experimental ratios of the diffraction from an ideal circle were measured for all peaks above 1 mm high.

$$c = \sum_{all\ peaks} \left(\frac{h_{m+1}}{h_m} - \frac{t_{m+1}}{t_m}\right)^2$$

Where the h_m were experimental intensity heights for a nuclear image and the t_m were the experimental ratios found from an ideal circle. These square differences were added together to give the chromatin differences (c) of each radial CCD scan. These differences were then added together to give the chromatin value (C) for that nucleus. The low chromatin values for the first three nuclei are because they are chromatin free. Much lower chromatin values can be obtained by using the average of the height ratios for these three chromatin free nuclei as the standard

height ratios instead of those calculated theoretically above. The chromatin values of the last three reflect Dr. Miles' feelings about the deformity of their chromatin texture. The last nucleus, among the lumpiest ever found, had a chromatin value over ten times larger than the others.

1.425) Pleomorphism

Pleomorphism is a pathologist's subjective estimation of the misshapenness and amount of straight edges of a nucleus. Edges scatter light in a radial spoke, which could easily be seen in the diffraction pattern of the small rectangular and triangular nuclei. Each time the chromatin variation c was calculated for a radius, the sum of the heights of the peaks was written down to be compared to those of the five other radii. The largest sum divided by the smallest sum was used to quantify pleomorphism. In the data tables these maximum and minimum values are listed under their columns. The small hexagonal, rectangular, and both triangular nuclei have two to 5 times higher pleomorphic values than the other ovals.

The pleomorphic nuclei of figures 1.10-1.12 have a normal intensity decay, indicating no chromatin clumping, but the variation of the distance between their first two minimums Δr_m indicates their pleomorphism. Therefore, another possible measure of pleomorphism would be the variation in the Δr_m used to measure area.

Figure 1.9a Photographs of (from right to left) small elliptical nucleus, its Fourier transform, and the six radial intensity traces of its transform every 30 degrees.

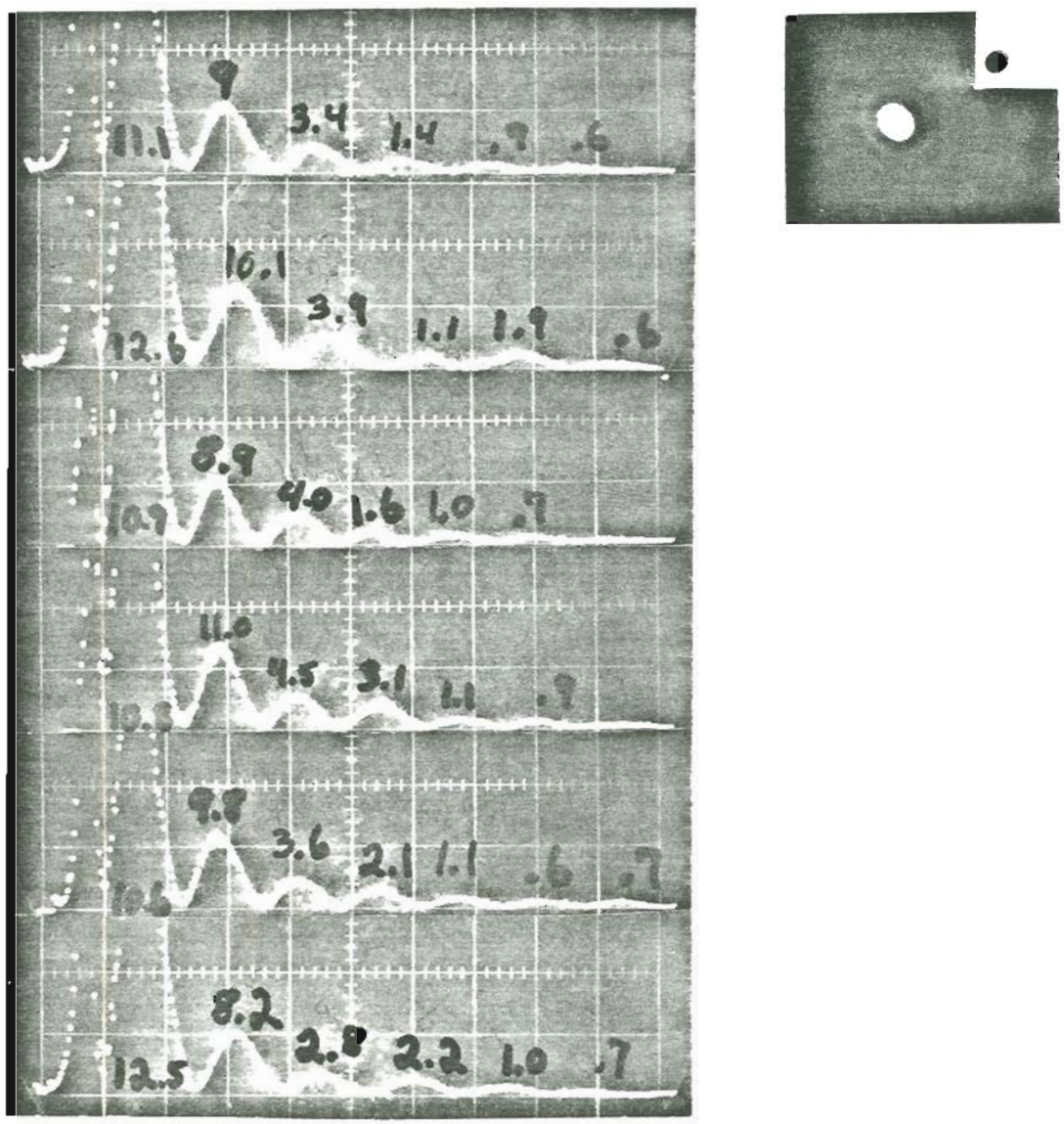

Figure 1.9b Table of data and derived values for the small elliptical nucleus.

Small Elliptical Nucleus						
sample angle =	0 deg.	30 deg.	60 deg.	90 deg.	120 deg.	150 deg.
$\Delta r_m =$	11.1	12.6	10.9	10.8	10.6	12.5
$h_2 =$	9	10.1	8.9	11.0	9.8	8.2
$h_3 =$	3.4	3.9	4.0	4.5	3.6	2.8
$h_4 =$	1.4	1.1	1.6	3.1	2.1	2.2
$h_5 =$	.9	1.9	1.0	1.1	1.1	1.0
$h_6 =$	.6	.6	.7	.9	.6	.7
c =	18	19	14.8	22.5	52	23.5
				max=20.6		min=14.9
Pleomorphism = 20.6 / 14.9 = 1.38				$C = \sum c_m = 91.3$		
Area = 4.67				Darkness = 1.06		

Figure 1.10a Photographs of (from right to left) small hexagonal nucleus, its Fourier transform, and the six radial intensity traces of its transform every 30 degrees.

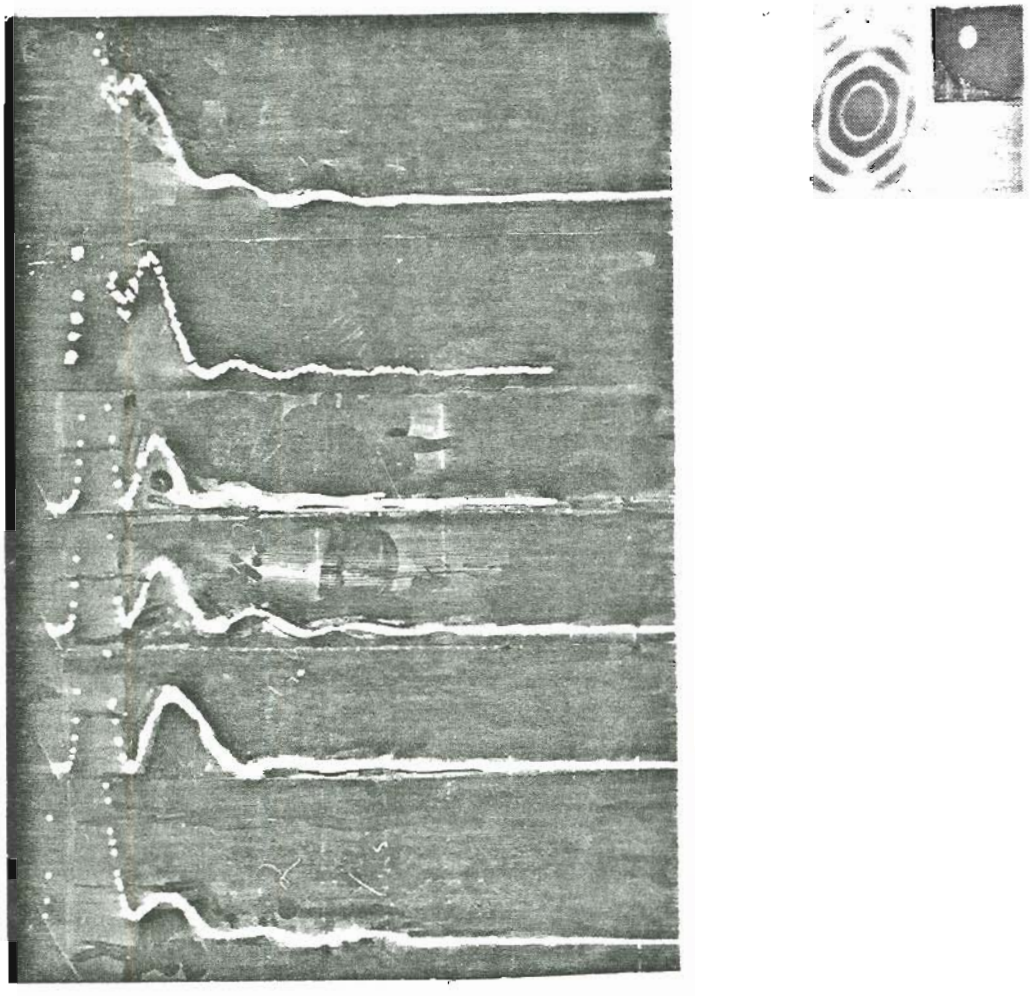

Figure 1.10b Table of data and derived values for the small hexagonal nucleus.

Small Hexagonal Nucleus						
sample angle =	0 deg.	30 deg.	60 deg.	90 deg.	120 deg.	150 deg.
Δr_m =	12	11.5	10	11	15	12.0
h_2=	4.1	1.7	2.4	4.3	1.0	2.0
h_3=	1.7	1.0	.9	1.7	.6	1.5
h_4=	.9	.5		.9		.8
c_m =	6.3	11.7	2.2	5.2	13	23
				max=6.9	min=1.6	
Pleomorphism = 6.9 / 1.6 = 4.3				C = $\sum c_m$ = 61.4		
Area = 4.42				Darkness = 1.29		

Figure 1.11a Photographs of (from right to left) small rectangular nucleus, its Fourier transform, and the six radial intensity traces of its transform every 30 degrees.

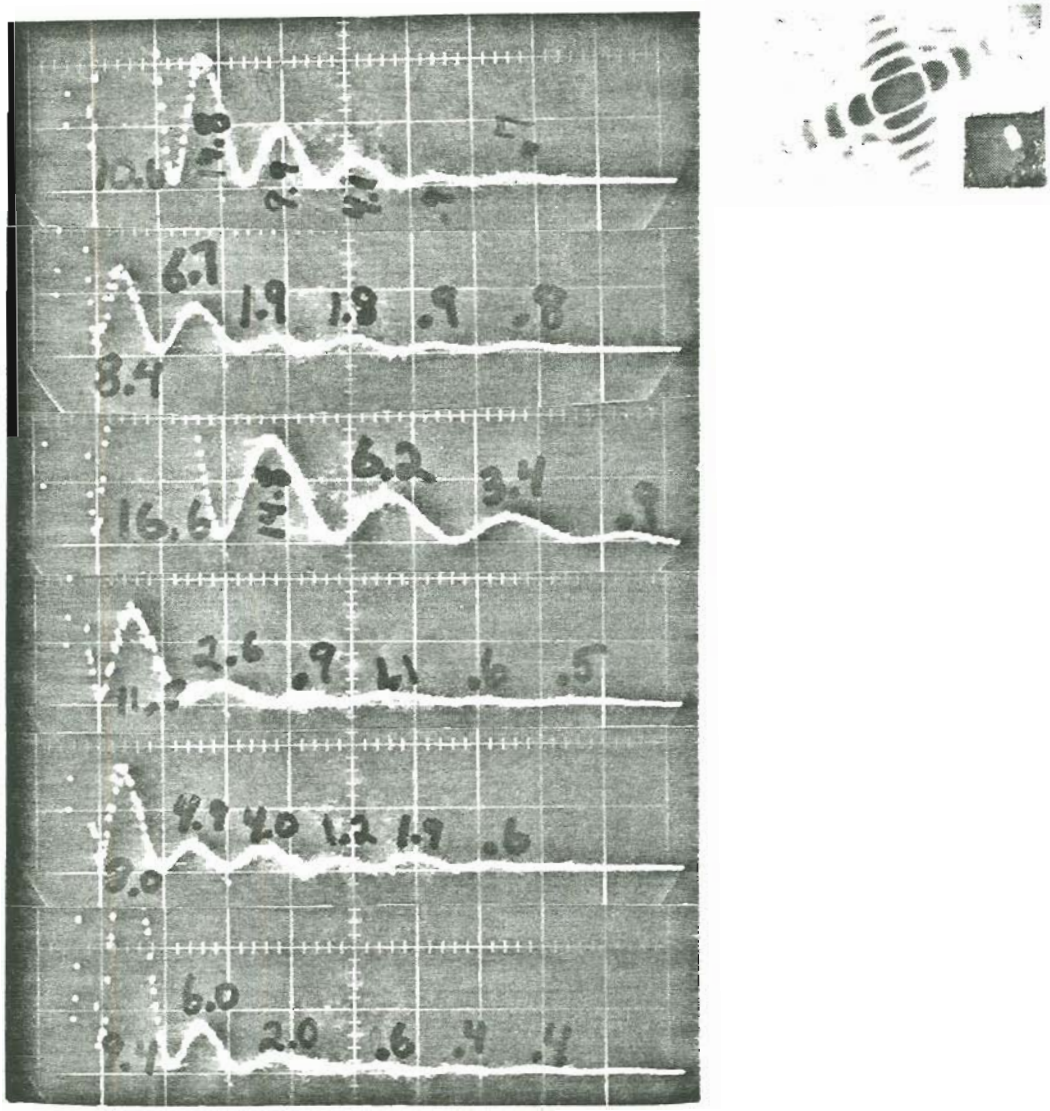

Figure 1.11b Table of data and derived values for the small rectangular nucleus.

Small Rectangular Nucleus						
sample angle =	0 deg.	30 deg.	60 deg.	90 deg.	120 deg.	150 deg.
Δr_m =	10.6	8.4	16.6	11.8	8.0	9.4
h_2=	17.8	6.7	14.8	2.6	4.9	6.0
h_3=	9.9	1.9	6.2	.9	4.0	2.0
h_4=	4.1	1.8	3.4	1.1	1.2	.6
h_5=	.9	.9	.9	.6	1.9	.4
h_6=	.7	.8		.5	.6	.4
c_m =	18	19	14.8	22.5	52	23.5
max = 31.4				min = 5.7		
pleomorphism = 31.5 / 5.7 = 5.5				C = $\sum c_m$ = 149.8		
Area = 6.1				Darkness =1.25		

Figure 1.12a Photographs of (from right to left) small triangular nucleus, its Fourier transform, and the six radial intensity traces of its transform every 30 degrees.

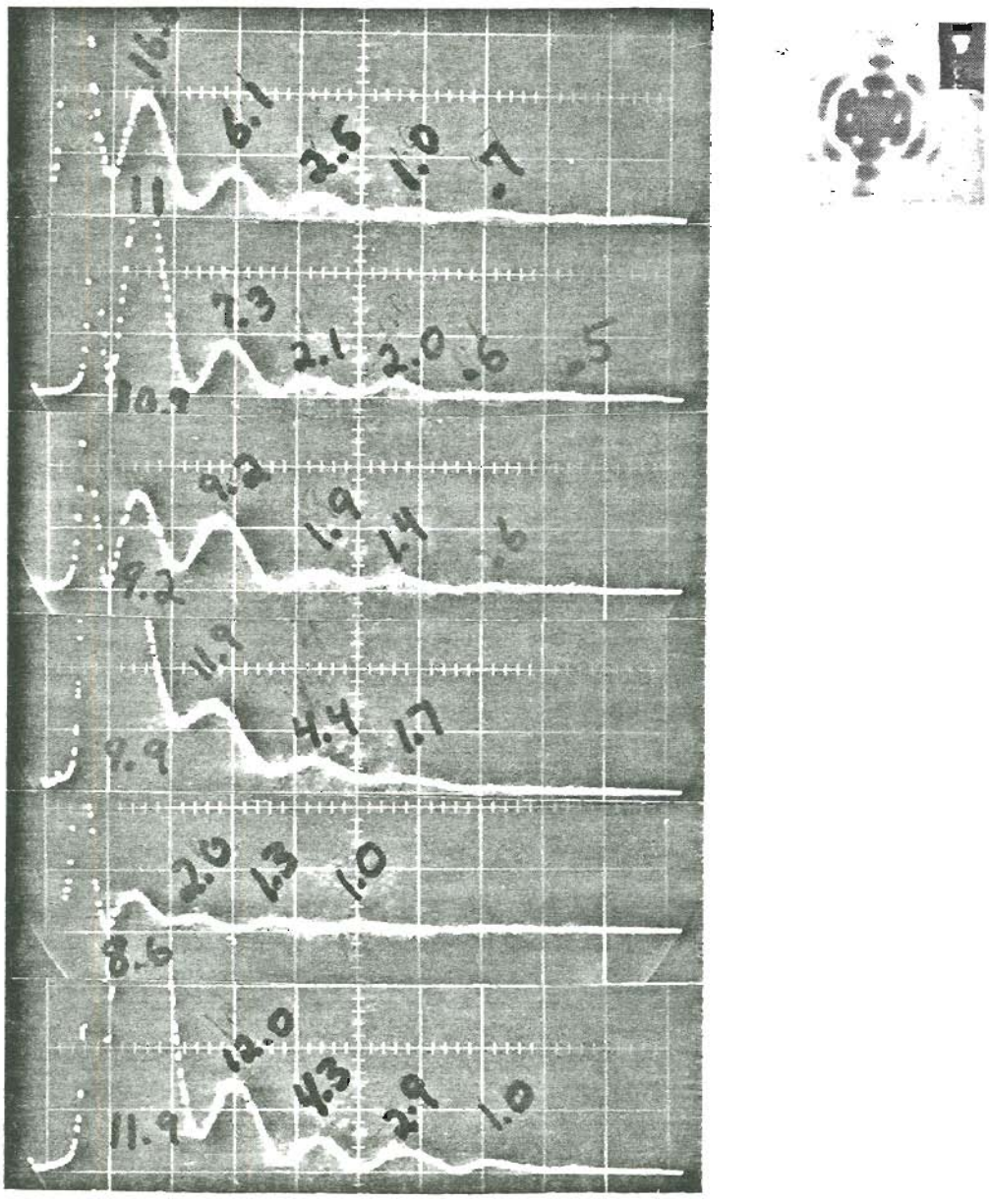

Figure 1.12b Table of data and derived values for the small triangular nucleus.

Small Triangular Nucleus						
sample angle =	0 deg.	30 deg.	60 deg.	90 deg.	120 deg.	150 deg
Δr_m =	11	10.9	9.2	9.9	8.6	11.9
h_2=	6.1	7.3	9.2	11.9	2.0	12.0
h_3=	2.5	2.1	1.9	4.4	1.3	4.3
h_4=	1.0	2.0	1.4	1.7	1.0	2.9
h_5=	.7	.6	.6			1.0
h_6=		.5				
c_i =	10	22.6	16.7	12.6	30	14.3
					min=4.3	max=20
pleomorphism = 20.2 / 4.3 = 4.8				C = $\sum c_m$ = 116.2		
Area = 6.0				Darkness = .84		

Figure 1.13a Photographs of (from right to left) large oval nucleus with coarse chromatin, its Fourier transform, and the six radial intensity traces of its transform every 30 degrees.

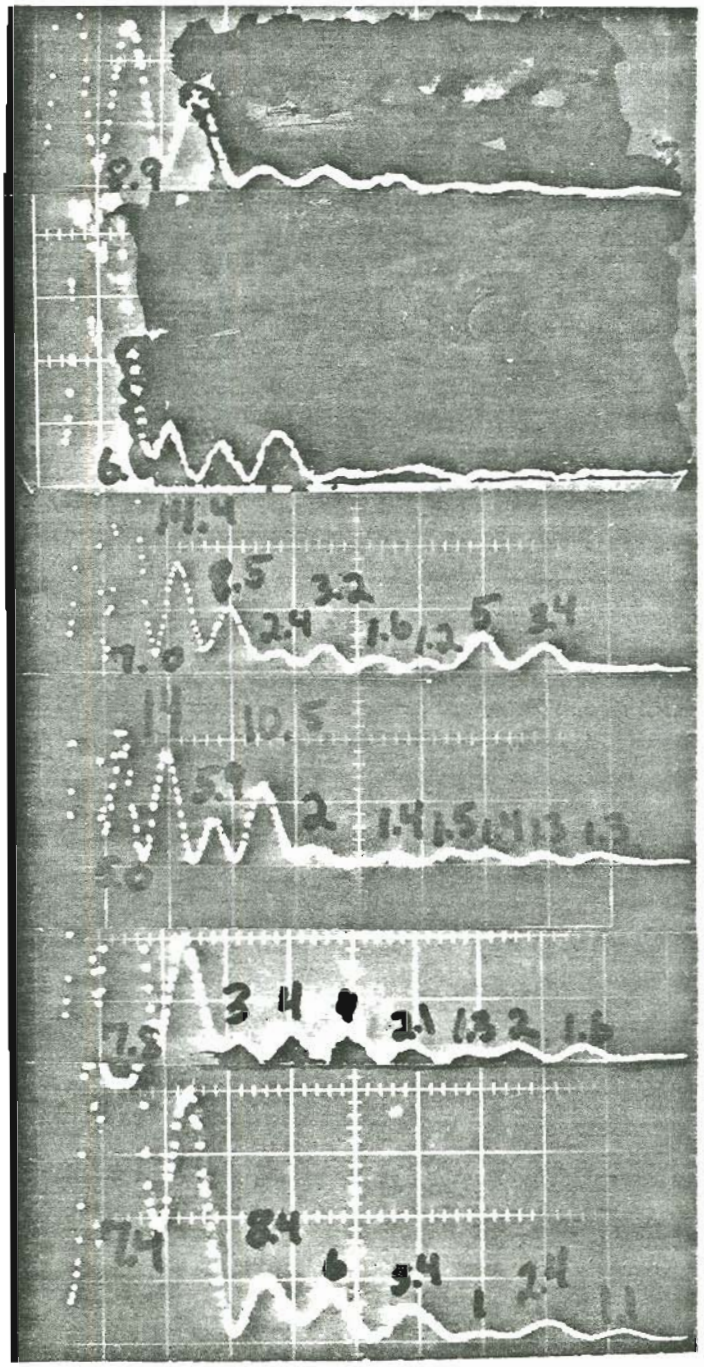

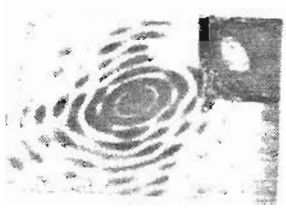

Figure 1.13b Table of data and derived values for the large oval nucleus with coarse chromatin.

Large Oval Nucleus with Coarse Chromatin						
sample angle =	0 deg.	30 deg.	60 deg.	90 deg.	120 deg.	150 deg.
$\Delta r_m =$	8.9	6.6	7.0	5.0	7.8	7.4
$h_2 =$	12.4	7.8	14.4	14	16.9	34
$h_3 =$	2.6	5	8.5	5.9	3	8.4
$h_4 =$	2.6	6.9	2.4	10.5	4	6
$h_5 =$	1.6	1.0	3.2	2.0	4.0	5.4
$h_6 =$	.7	1.5	1.6	1.4	2.1	1.0
$h_7 =$	1.0	.6	1.2	1.5	1.3	2.4
$h_8 =$	.3	.8	5	1.4	2	1.1
$h_9 =$	.8	.6	3.4	1.3	1.6	
$h_{10} =$				1.3		
$c_m =$	24	61	36	44	40	29
min=24.2						max=58
pleomorphism = 58 / 24.2 = 2.4				$C = \sum c_m = 234$		
Area = 13				Darkness = 2.0		

Figure 1.14a Photographs of (from right to left) large triangular nucleus with coarser chromatin, its Fourier transform, and the six radial intensity traces of its transform every 30 degrees.

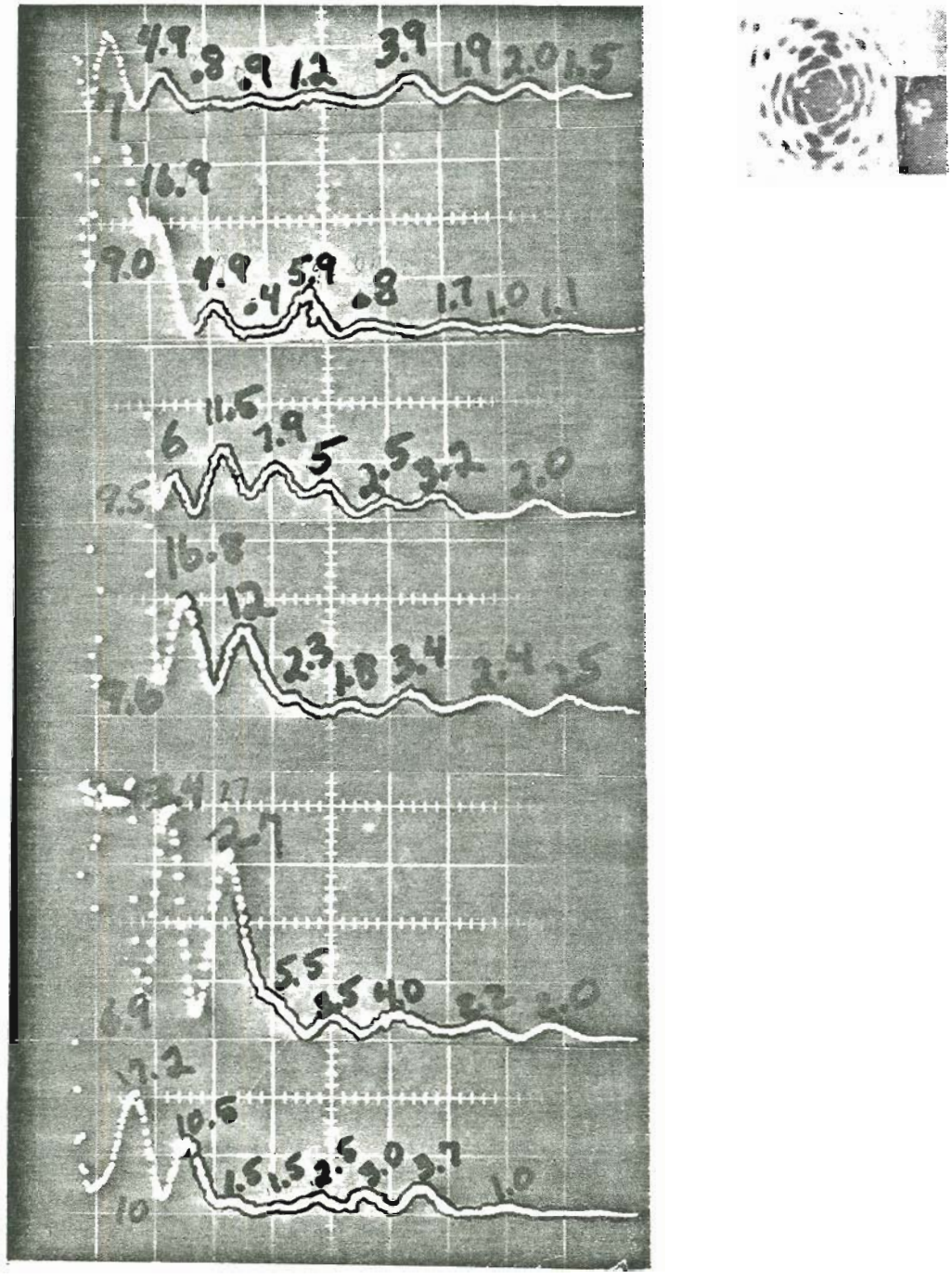

1.5) Discussion

The parallel processing ability of optical Fourier transforms has been used to simplify the reduction of the statistical data of nuclear images. This allows estimates of size, shape, darkness, and texture to be made of each nuclear image with a simple calculation. This ease occurs because the only required data, the radius of the first two nulls and the heights of the diffraction rings, can be easily obtained from the raw intensity data by looking for zero values and zero slopes. These few values, because of the translation invariance of the Fourier transform, can always be measured from a coordinate system fixed on the optical axis.

However, there are several approximations made to achieve these estimates, and six nuclei are too few for a thorough test. But it is important to try to measure these classical clues, because they mean so much more to pathologists than spatial frequencies do. Previous researchers [6] had too much data and too little knowledge that fit into the pathologist's culture, or they [9] had only verbal descriptions of "spikes" from misshappen pleomorphism or "mottled appearance" from chromatin.

The major problem preventing implementation of this near real-time hybrid device is the requirement of a photographic input instead of the actual cell. A solution other than an unsatisfactory Liquid Crystal Light Valve is actively being researched, but because of the particularly high data rates required for microscopic image analysis, there is little chance of using a coherent light valve to photograph the cells rapidly enough.

Since we are only interested in the real-valued intensity of the image, a way may be able to be found which ignores the optical phase variations of an actual

cell. This would make a coherent light valve unnecessary. The next chapter investigates this possibility.

Chapter II

OPTICAL ANALYSIS OF INCOHERENT MICROSCOPE IMAGES

Abstract

The geometric and holographic methods of phase incoherent optical processing were investigated for pattern recognition of real-time, diffuse microscope images. The theory and implementation of these processors is discussed in view of their mutual problems of dimness, image bias, and detector resolution.

The dimness problem was solved by either using a holographic correlator or a speckle free laser microscope. The latter was built using a spinning tilted mirror which caused the speckle to change so quickly that it averaged out during the exposure.

To solve the bias buildup problem low image bias template patterns were generated by four techniques labeled here as: microphotography of samples, creation of typical shapes by computer graphics editor, transmission holography of photoplates of samples, and by spatially coherent color image bias removal. The first of these templates was used to perform correlations with bacteria images. The aperture bias was successfully removed from the correlation with a video frame subtractor.

To overcome the limited detector resolution it is necessary to discover some analog nonlinear intensity peak detector, such as optical bistability. Without such

a device, the output detector must sample many points of the correlation to determine whether there is a good correlation anywhere. An analog nonlinear intensity peak detector would allow one detector sampling point to determine if the correlation intensity was high anywhere in the correlation output, that is, for any separation of the correlated functions.

Three specific medical uses for the intensity correlators are presented.

2.2) Theory of Incoherent Optical Information Processing

Coherent image processing performs a full Fourier transform on its input image. Non-transparencies (such as a printed page, CRT, or any real image) have a random phase function that multiplies the transmittance which usually contains the valued information. When transformed, the transform of the random phase function (speckle) is convolved with the transform of the transmittance amplitude of interest, making it undetectable.

Incoherent image processing is sensitive only to the intensity of the image, and so the random phase function of non-transparent images is ignored. This ability to use such inputs as a printed page, CRT, or any real image greatly enhances the usefulness of the system. However, as will be shown, the problems of bias, light throughput, and detector resolution hinder the application of incoherent image processing's full powers.

Unlike the highly collimated light of coherent optics, incoherent inputs theoretically need to send light out equally in all directions, but usually a narrow cone centered perpendicular to the plane of the input diffuser is all that is uniform. Our diffusers fulfilled this function well for a cone angle of about 10 degrees. A CRT works much better, putting light out in all directions almost equally.

Space bandwidth product (SB) is a measure of the maximum data storage capability. A 100 line per mm grating can be thought of as a bit stream in which individual grating lines could be turned on or off. If a 100 ln/mm lens is good over a 10mm field of view then each dimension of its image could store no more than 1000 points. A square image with 10mm sides (1000 points) could store one million points in a checkerboard data page.

Space bandwidth frequency (SBF) is an even more significant figure of merit for data processing ability, since the shorter the data processing cycle, the better the device performance. Image processing systems produce very high SBF quality values because light moves 30cm in a nanosecond.

An excellent review of intensity correlators is given in [16] and in [17]. A few of the important types will be discussed here.

The simplest incoherent optical processor is the scanning correlator. Here the input is imaged onto the template. Either image is then moved to change the Δx of the correlation and the total amount of light passed is detected by a photocell. The drawback of this technique is that mechanical scanning is required, but this scanning may already be provided by some moving systems, such as a spinning optical memory disk or a flowing cell analyzer.

2.1) Shadow Casting Geometrical Correlators

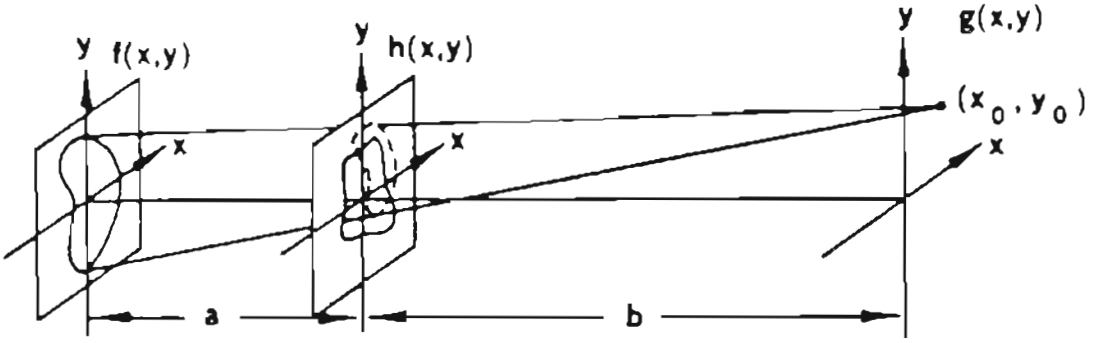

Figure 2.1 Basic geometry for shadow casting correlator.

The simplest nonscanning correlator is shown in figure 2.1. It was first proposed by Bragg. [1] Geometrical rays of light emanate in all directions from the input f(x,y). All light that arrives at a point (x_o,y_o) in the correlation plane g(x,y) had to go through the template h(x,y). If the input is similar to a properly scaled and rotated version of the template, then a maximum of light intensity will be found at a point (x_o,y_o) in the correlation plane whose coordinates correspond to the separation which makes the correlation of f and h a maximum. In our study the template was always the negative of the object to be detected, so a minimum of light intensity was sought.

The literature gives scaling relationships for shadow casting correlators as: [18].

$$g(x_o,y_o) = \int\int_{-\infty}^{\infty} f\left(\left(x - x_o\frac{a}{a+b}\right)\Big/\frac{b}{a+b}, \left(y - y_o\frac{a}{a+b}\right)\Big/\frac{b}{a+b}\right) h(x,y)\, dxdy$$

The best way to understand the scaling of this system is by thinking of point sources as delta functions. Correlation with a delta function returns just the origi-

nal function. A delta function (pinhole) as input is a point source projector. See figure 2.2. A delta function in the template is just a pinhole camera. See figure 2.3. A geometrical correlator is a combination of the two.

Figure 2.2 is a point projecting a shadow of the template onto the correlation plane.

Point Projector

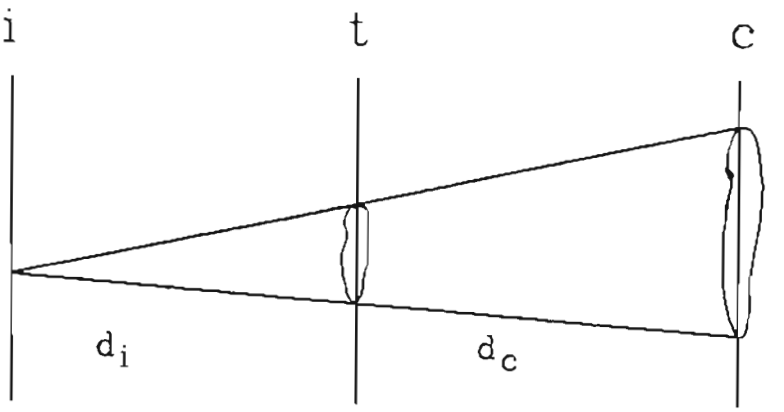

$$M = \frac{\text{projected image size at correlation plane}}{\text{template size}}$$

$$= 1 + \frac{d_c}{d_i}$$

Figure 2.3 is a pinhole camera made with a delta function (pinhole) in the template.

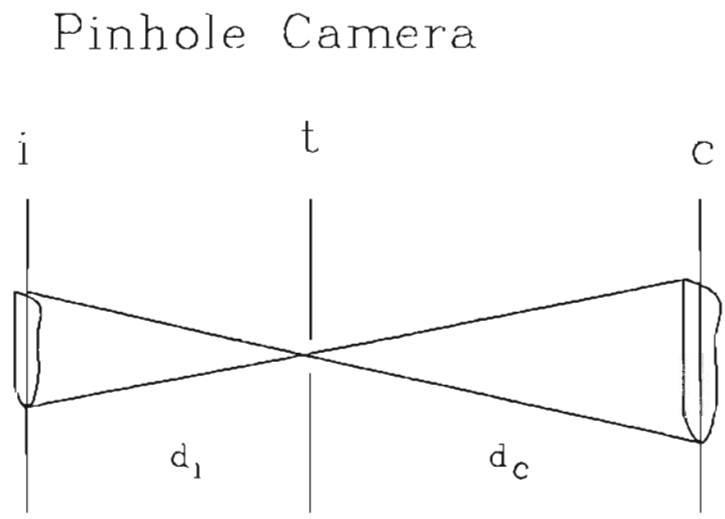

$$M = \frac{\text{image size at correlation plane}}{\text{input size}} = \frac{d_c}{d_i}$$

The pinhole camera and projector can be used to explain correlation. Imagine two pinholes were the input of the pinhole projector instead of one; the two images of the template would be cast onto the correlation plane. Likewise, two pinholes in the template would give two inverted images projected onto the correlation plane.

For a superposition of input points you would get a correlation of the input with the template. Thus each point of the input or template has the other's image superimposed on it. This duality is an illustration of correlation's mathematical commutability.

In practice our templates were high contrast photographs usually held directly against a single lens reflex camera body in the same way as a lens would normally be used. The correlation plane was the film plane, and the correlation could be seen through the viewfinder or exposed with the normal shutter action.

Proper scaling was found by putting an aluminum foil pinhole alternatively in both the input and template planes, and by moving the object towards or away from the camera and template until the two images being correlated were in proper scale. Usually a pinhole was used in the template to act as a camera to show the input scene next to the two dimensional correlation patterns. Figure 2.18 has one of these pinhole cameras in its correlation.

Although this simple lensless projection described above was found to be most useful by this thesis, the usual method of geometrical "template matching" involves a lens. With such a lens setup, no two of the three input, template, and correlation planes are in a normal image relationship. Most of the geometrical correlator research (to be described in the next few paragraphs) has been done with lens correlators, for a reason not explained in their papers nor understood by this thesis. Lens correlators usually suffer from the aberrations and limited space-bandwidth of the lens. Worse however, is that use of a lens usually results in different parts of the template seeing different parts of the input image. That is, the input is not the same for all parts of the template. While this problem has been

ignored by previous researchers, the reader can investigate this problem with a careful ray tracing to show that the input function remains the same over the entire correlation plane only if the template is held directly against an ideal thin lens.

In a recent letter, [19] scaling relationships were derived for this general type of lens based correlator by the same method as used in this thesis: inserting pinholes in the input and template planes and determining the sizes of the images.

The second of these lens correlator papers [20] pointed out that, just as in coherent spatial filtering, incoherent correlation peaks may be allowed to pass on through the rest of an optical system to reconstruct an image of the input and template superimposed. This is best understood by thinking of the correlator as an imaging system. The smaller the aperture around the correlation peak, the larger the depth of focus of the imaging system, and the sharper the two images of the input and template can be focussed simultaneously.

The effect of diffraction on resolution was studied by the third author, [21] who showed that the number of analog multiplications was proportional to the number of degrees of freedom of a light beam (= aperture area x solid angle / square of wavelength). He also showed that the number of resolvable directions increases with the separation of the transparencies at the cost of including fewer products in each summation approximating the correlation function. Although he worked with lens correlators, the results appear to hold for lensless correlators, with the aperture stops of the system being the apertures of the input and template.

Green was the only author to give an example of correlation, and his was an academic five pointed star. None of these three authors mentioned methods of preparing templates, reducing bias, or increasing light throughput.

2.2) Holographic Correlators

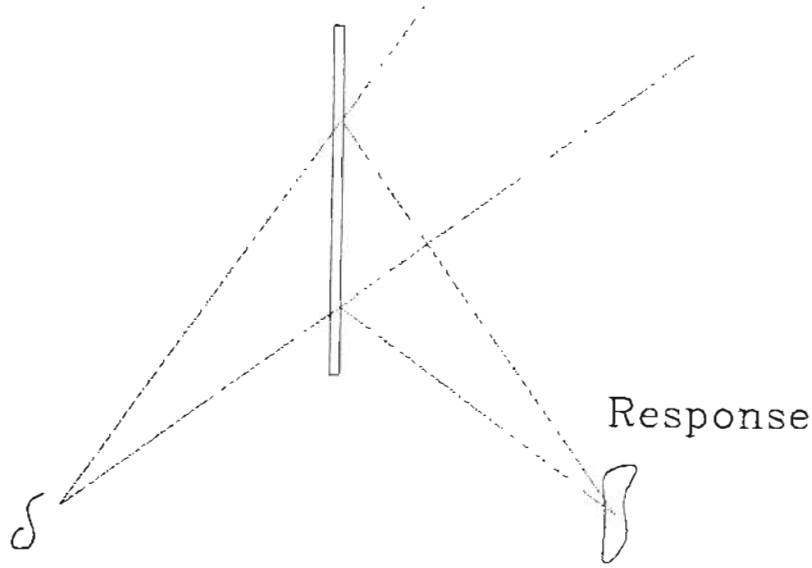

Figure 2.4 Holographic correlator

A major breakthrough was made in 1968 when A. Lohman used holograms as incoherent correlators. [22] Basically, the hologram's image shown in figure 2.4 can be thought of as the impulse response of a linear system to the reconstructing point source which acts like a delta function. If the reconstructing source is an extended source rather than a point impulse, then the output of the hologram is the correlation of the hologram's image with the input. This is why holograms blur when reconstructed with diffuse lights; the image of the diffuse source is superimposed onto each point of the reconstructed image. Once again, there is a bias problem since the intensity impulse response of the hologram must be positive everywhere.

When light propagates from the input image to a distant hologram or lens, the Huygens-Fresnel principle implies that the image is Fourier transformed. [23] Since the hologram records and manipulates information in this frequency domain, the correlation spoken of above must correspond to a multiplication of the hologram with the transform of the input image. This is indeed what a transmittance function does to the light going through. Correlation is physically realized by multiplying light intensities with transmittance values in the frequency domain.

Figure 2.5 Example of holographic impulse response

The figure 2.5 is a 2X image of the response of a transmission hologram made by a PAAP developer with bromine bleach. [24] This unique holographic developer uses ascorbic acid to reduce the latent image silver without releasing reaction products which oxidize and harden the gelatin emulsion. The addition of a small amount of silver-halide solvent (.5g/l ammonium thiocyanate) allows for the unexposed silver halide to be dissolved and precipitated onto the fringes as reduced silver.

The hologram produced by this method had an 11 percent diffraction efficiency and good image quality. Along with the nuclear images is a 100 dot/inch halftone screen for image quality investigation. Both reference (input) and object (correlation) beams were 500 mm away and 45 degrees to the 2.5"X 4" holographic plate.

Holographic correlators have been of more recent research interest than geometrical correlators have. A.W. Lohman launched the field with two pioneering papers. The first, labelled "Matched Filtering with Self-Luminous Objects", was a difficult to understand theoretical work, probably because the concept was still so intertwined with the concept of the coherent matched filter. [22] By the second paper, [25] he made two suggestions to solve the bias and light throughput problems. The first was "suppression of the useless low spatial frequencies ...for better target discrimination." The second was imaging the input source onto the input, for example onto an opaque print, in order to increase the input intensity.

The next paper was by Bieringer, "Optical Correlation Using Diffuse Objects". [26]. Its major contribution was an indication that this application of linear system theory could be applied to all off-axis, diffuse object beam holograms, although he did not use the equal reference and object angles that were found necessary in this thesis. This paper was very useful for this thesis because it correlated arrays of circles and lines (figure 5 of his paper), which looked similar to the microscope photoplates used in this thesis.

Maloney published two works in 1971 [27] the first, "Lensless Holographic Recognition of Spatially Incoherent Patterns in Real-Time" used multiple, spatially offset holograms to recognize code features in alphabetic letters. The

features were small pieces of a letter, so the author could avoid discussing the bias problem. This paper described the first peak-detection scheme using detectors behind pinholes. This technique gives up shift invariance, i.e. the correlation spike moves off the pinhole if the input shifts. His second paper "Real-Time Holographic Filtering of Oscilloscope Traces" [28], applied the same optical processor to input from an oscilloscope CRT. He was the first to use CRTs with phosphors emitting narrow spectra. This was necessary since he was using a holographic correlator.

"Direct Matched-Filtering of Pen Recordings Using Sodium Light", [29] used the paper output of an EEG machine illuminated with sodium light for input. Using this raw input, the device was capable of recognizing a certain brainwave pattern. The major contribution in this paper was the use of the negative of the function to be detected as the template to greatly reduce the bias. This thesis generalized this bias reduction technique to color inputs.

Finally in 1983, after this thesis' work on incoherent correlators was well under way, a group of five authors published a holographic incoherent correlator system for industrial pattern recognition of hand tools. [30] They lowered the correlation bias with an electronic time differentiation of the input video signal. This novel solution worked well for vertical edges, but not as well for horizontal edges, since the time derivative of the video signal would not pick up horizontal lines as sudden edges. The template images were created by the same technique, and photographs of their video display were taken. Transmission holograms in dichromated gelatin were made of these photographs and put on a rotating wheel in front of a narrow band phosphor CRT. The correlation was detected with a video camera.

2.21) Scaling in Holographic Incoherent Optical Information Processing

When a hologram of an object is reconstructed by another object which is being used in the location of the original reference beam, the reconstructed image will be the correlation of the original object used to record the hologram and the object currently being used to reconstruct the hologram.

As long as the hologram is thin enough to still reconstruct, an angular deviation about the reference translates into an angular deviation about the reconstructed image angle. Perpendicular to the plane formed by the reference and object beams, these angles are always equal, but in this plane we must derive the exact displacement by starting with the grating equation:

$$\sin\Theta_r + \sin\Theta_o = \frac{\lambda}{d},$$

where Θ_r and Θ_o are the reference and object beam angles relative to the hologram perpendicular. Applying the differential operator $\frac{d}{d\Theta_r}$ yields:

$$\cos\Theta_r + \cos\Theta_o \frac{d\Theta_o}{d\Theta_r} = 0$$

Therefore rearranging,

$$\frac{d\Theta_o}{d\Theta_r} = \frac{-\cos\Theta_r}{\cos\Theta_o}$$

So long as the hologram is made with $\Theta_o = \Theta_r$, the angular deviations are equal (but opposite).

The size of the object and reference displacements Δs_o and Δs_r divided by the distance to them from the hologram are the angles which are equal.

$$\frac{\Delta s_r}{d_r} = \frac{\Delta s_o}{d_o}$$

If they are different sized images of the same object, "being in scale" means that translation of the reference object by a distance equal to its size will cause a translation of the hologram's image by a distance equal to its size. We can then set $\Delta s_o = s_o$ the object size and $\Delta s_r = s_r$ the reconstruction object (input) size.

$$\frac{s_r}{d_r} = \frac{s_o}{d_o}$$

The hologram was originally exposed with a certain object size s_o a certain distance d_o away. These give us the input distance d_r needed for any given reconstruction size s_r which may be varied. In terms of the microscope magnifications used to create both images this becomes:

$$\frac{m_r}{d_r} = \frac{m_o}{d_o}$$

So if the hologram was made of a transparency 10 cm away which is a 100X magnification microscope image, a 200X input image used to reconstruct the hologram should be 20 cm away to keep the images in scale. The original hologram should be made with this reference distance. If the reconstructing input must be a different distance away than the original reference, then the hologram's output image location will change. A hologram of a real converging image can be thought of as a lens, and the thin lens equation is useful for figuring image positions if the reconstruction distance changes. The focal length of the hologram corresponds to how fast its spatial frequency changes when moving in a radial direction from the optical axis and is inversely dependent on the wavelength used. [31]

2.23) Light Throughput

The parallel way incoherent processors work necessitates that light emanate from the input object in all directions, since all template images must receive some light. One of the drawbacks of geometrical templates is that light can go through only where there is some transmittance, and there isn't much of it when using the usual opaque template with small clear images as in figures 2.5 and 2.16. This means very little light gets through the small template images to reach the detector. One of the advantages of the holographic system is that light hitting the entire area of the hologram is used to make a consequently high intensity impulse response. However, a problem with holograms is the low diffraction efficiency (10-20 percent) of most high signal to noise ratio silver halide holograms. For all holographic materials there is an inverse relationship between diffraction efficiency and signal to noise ratio, and dichromated gelatin is the only material capable of 50 percent diffraction efficiencies at a 50 to 1 signal to noise ratio. [32] Dichromated gelatin unfortunately requires very careful preparation, exposure, and processing [33] with techniques that must be taken solely from the literature, since there are so few active researchers. The literature techniques must be modified for each laboratory's humidity, gelatin, and processing need. [34] More information on dichromated gelatin, including a favorite technique, can be found in appendix G.

Figure 2.6 Bias problems in incoherent OIP

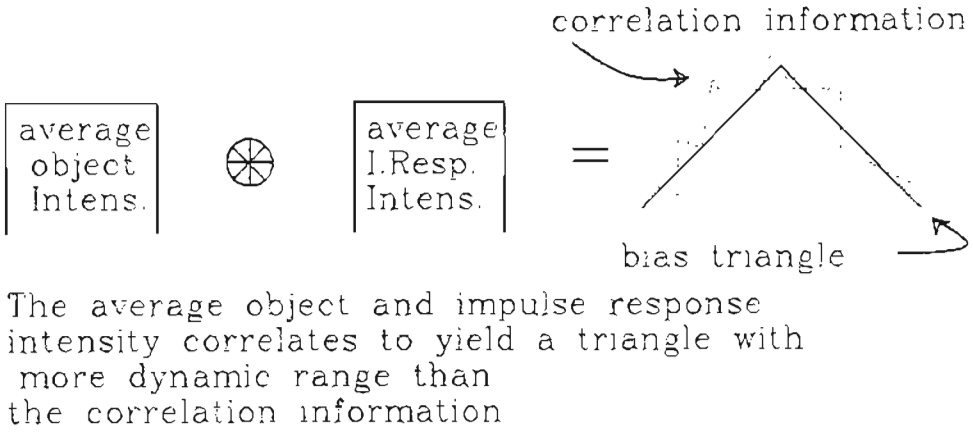

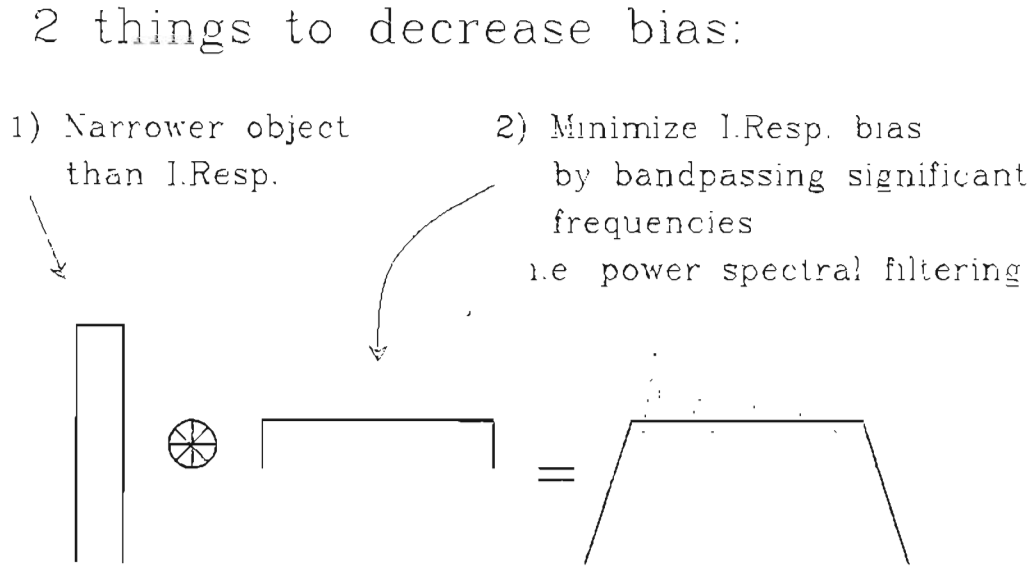

2.24) Bias Reduction

The bias problem of phase incoherent processing is illustrated by figure 2.6. Since both the object and template must have non-negative transmittances over their entire surface, if you integrate them there is a net bias to each one. When these average values are cross-correlated, they yield a triangular shape with more dynamic range than the correlation information. A more realistic waveform is shown dotted over the bias triangle.

Narrowing the size of the input is a good way to make the bias cross-correlation have a constant value which can be subtracted out globally from the entire correlation. [35] The bias subtraction discovered in this thesis (see section 2.35) is similar, but involves a more sophisticated pointwise subtraction of the bias function instead of a bias constant. However, in both cases the dynamic range of the detector is still wasted.

Another solution, proposed by Lohman, is to minimize the impulse response bias by putting the template transparency in a Fourier transform diffractometer and blocking the undiffracted light in the focal plane. [25] Since this undiffracted light corresponds to very low spatial frequencies in the image, this has the effect of edge enhancing the resultant image. This image could then be made into a hologram.

A still better solution is to bandpass only those spatial frequencies which are most characteristic of that class of object and which are different from the background noise. Most natural signals have a 1/f type power spectrum, [36] so most of the bias can be eliminated by blocking the low frequencies. This explains why edge enhancement had been found to be useful by Lohman.

The work with Dr. Miles, discussed in the first chapter, has shown that information about the size and shape of human nuclei is contained in the middle frequency range, and that the high frequencies contain the texture information. It is emphasized in this thesis that bandpassing these spatial frequency ranges when generating the template makes the correlation process a Weiner power spectral filter as well. [5] This is the old trick of bandpassing the signal to reduce the noise.

2.241) Spatial filtering

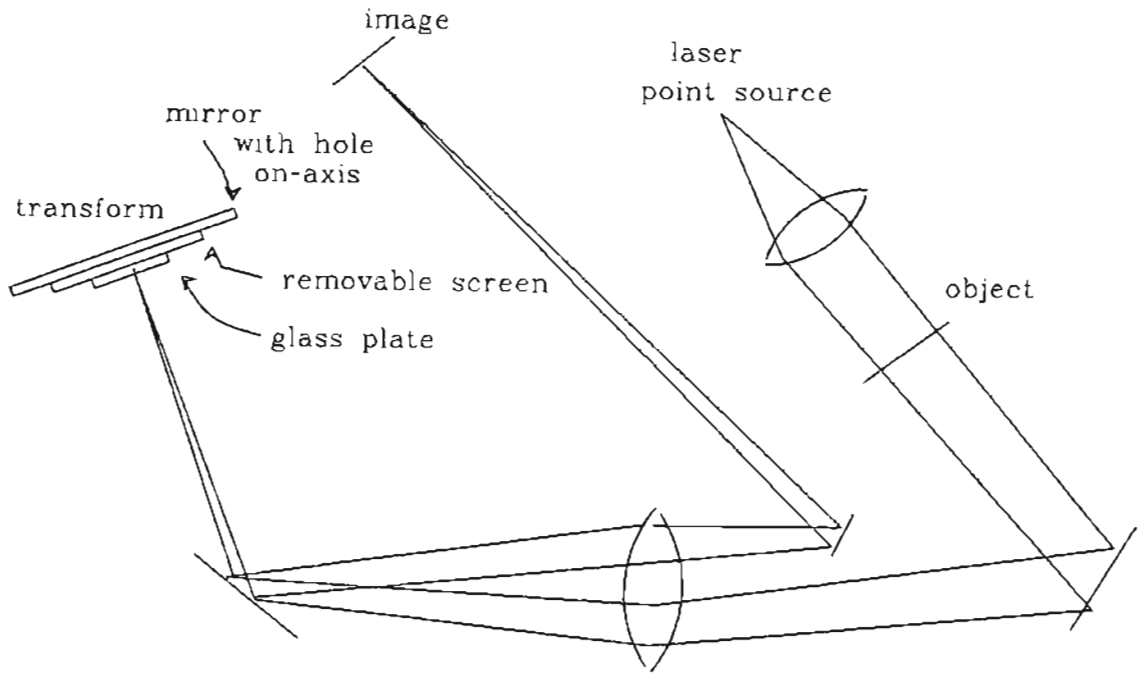

Figure 2.7 Handy spatial filtering setup.

A transparent image of the nuclei is put into a Fourier Transform diffractometer. [5] Most optical transformers are spread out in a line, and with long focal length lenses it is impossible to see the object, transform, and image planes simultaneously. The folded setup shown in figure 2.7 was developed to make spatial filtering more convenient. It has all three planes within arms reach, and uses only one expensive transform lens instead of the usual two. A portion of the object transparency can easily be moved over to the input aperture while examining its transform projected onto the screen. The transform can be easily filtered by drawing on the glass plate with a black pen to block unwanted spatial frequencies. Upon removal of the viewing screen, the transform reflects off the mirror, goes

back through the transform lens, and the re-transformed, filtered image is projected onto the screen where it can be examined with a hand-held magnifying glass.

The transform mirror has a small hole drilled into its center so the intense spot of on-axis undiffracted light, which corresponds to the bias, is not reflected back into the image. A hologram is then made whose impulse response is the edge enhanced image. This one-lens folded technique suffers slight aberrations due to the non-paraxial rays, so it is best for explorative work only.

The phase noise of the photographic film emulsion necessitates use of a liquid gate. [13] Xylene or mineral oil was so difficult to use that a number of alternatives were investigated, and complete success was found by cementing the transparency between two glass microscope slides with light curing epoxy. [14]

Figure 2.8 20X Magnification of coherently edge enhanced images.

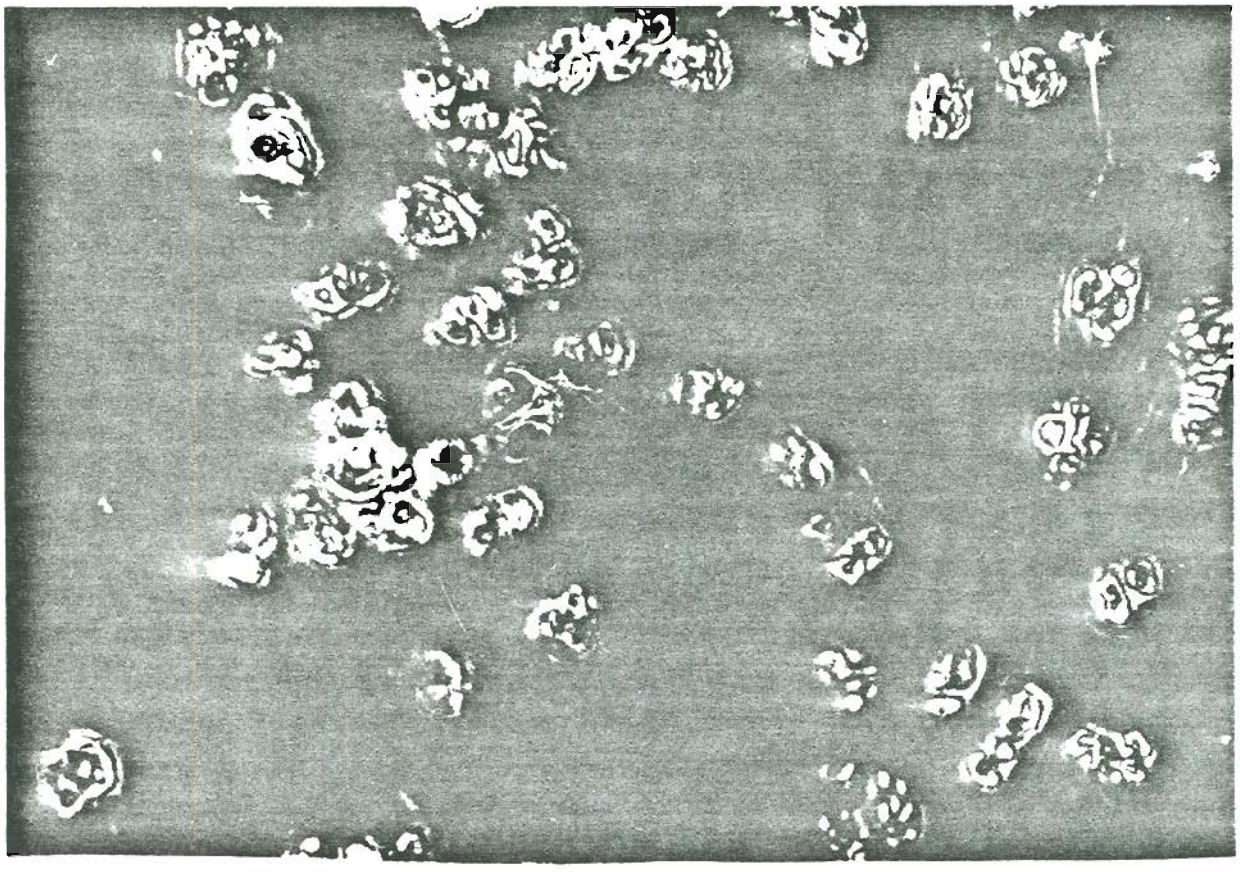

Edge enhanced nuclear images, made on a normal Fourier transform diffractometer, are shown in figure 2.8. Compare them to those in figure 1.4. Too much bias was removed and artificial edges were created. It was impossible to continuously vary the bias, because a hole in the mirror does not have a continuous variability. Ideally, a liquid crystal light valve could be used in the transform plane. This $50,000 device is manufactured by Hughes Aircraft and is capable of

real-time electronic photography. [37] This would allow any bandpassing function to be written onto the light valve by exposure with a cathode ray tube. Since only one light valve would be needed in the lab to make the mass-producible templates, the high cost of such a device would not be prohibitive. However, as will be discussed later, there is plenty of time to bandpass the template with a computer, since time must also be taken to develop the template into a transparency. It is the correlation of the input with the template that is rapidly processed optically.

2.242) Color Edge Enhance

As the microscope research progressed with clinical tissue, it became clear that color was essential for differentiating the biological images. Red blood cells are the same size and shape as human nuclei and only slightly larger than bacteria. In a monochromatic system, such as the 514nm laser microscope (discussed later in section 2.311), they are very difficult to distinguish. Using color makes it easier to distinguish the red blood cells from both bacteria and nuclei which stain blue. The geometrical method can, in theory, work just as well using color transparencies as templates, but there have been no attempts in the literature to use color slides directly as templates. Since they would still suffer from bias buildup, attempts were made to lower the bias of color slides (edge enhancement).

A tungsten iodide incandescent bulb (high brightness) is imaged onto a pinhole, so only the brightest point of the filament is passed as a uniform, spatially-coherent, white light beam. This beam passes through the transparency

Figure 2.9 Setup for coherent color edge enhancement.

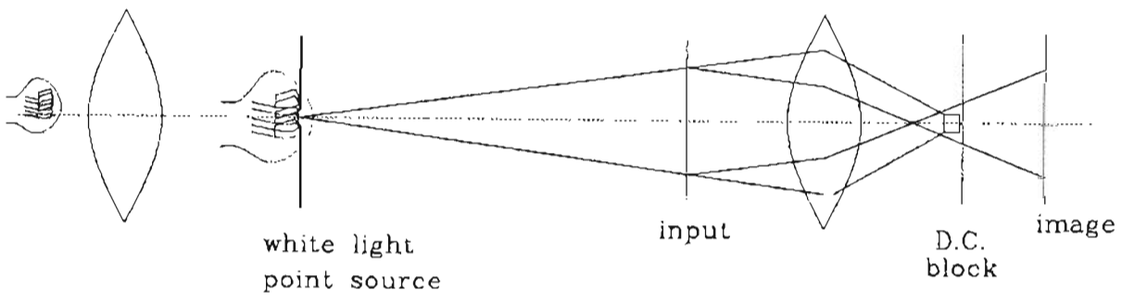

to be filtered, which is epoxied between glass slides to eliminate phase distortions. This slide is imaged by a projector lens onto the color film. In the focal plane of this lens a small (about .5mm) opaque dot is positioned carefully to block the undiffracted light that constitutes the bias of the image.

An example of an edge enhanced color 35 mm slide is shown in figure 2.11. The original photograph is shown in figure 2.10. Note how dark the background hills or the bricks of the wall are. The yellow strip around the sign in the upper corner shows the spatial period corresponding to the inverse of the diameter of the spatial frequency block in the focal plane. The spacing of the stones of the white building in the background matches this spatial period. This white light coherent

Figure 2.10 Initial image

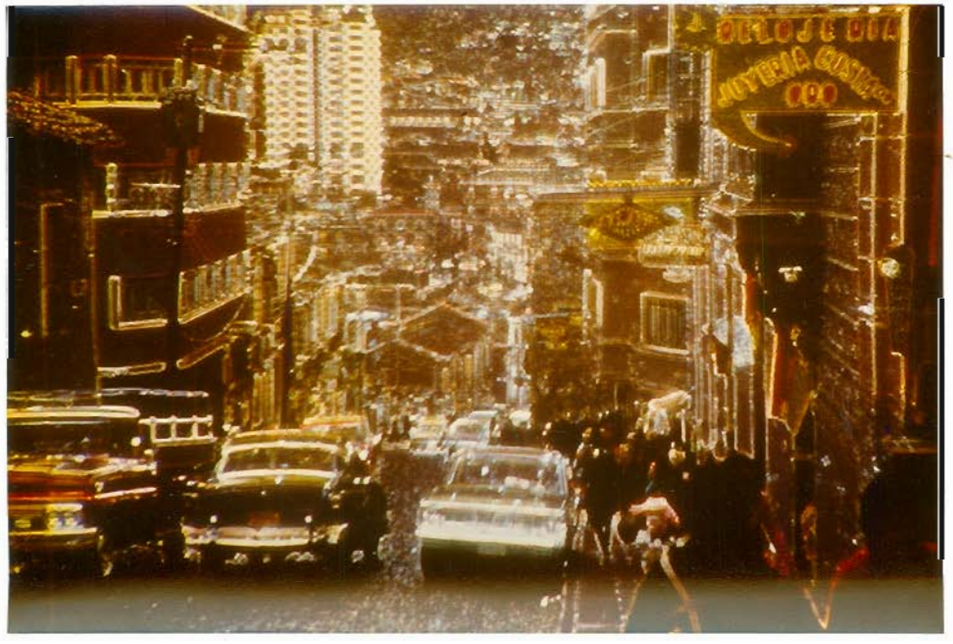

Figure 2.11 Low spatial frequency blocked image

2.3) Experiment

2.31) Microscope set-up

High power microscopes must be used to magnify the nuclei or bacteria to a size that incoherent optical processors can use. The quality of the input image depends on understanding how to build a good microscope.

A fundamental relationship in microscopy is the uncertainty principle $\Delta p \ \Delta x \geq constant$. To improve resolution ($smaller \Delta x$) requires a lens of high numerical aperture which brings light in from a wide angle ($large \Delta p_x$) . For maximum resolution an oil immersion lens and condenser are used. Our condenser was a hemispherical lens oiled against a diffuser which was against the bottom of the microscope slide. The diffuser serves to reduce "coherent artifact noise" by randomizing the light rays' directions and filling all the imaging channels. A condenser iris allows the numerical aperture of the illuminating light to be kept the same as the objective, ensuring the best contrast with no sacrifice in resolution. [38] The distance to the objective's image plane must be close to the 160 mm for which the aberrations of all microscope objectives have been corrected. Older objectives and eyepieces, such as the ones used in this study, must also be from the same manufacturer, since they correct each other's aberrations.

2.311) Speckle Reduction in Laser Microscopy

Because of the low light throughput problem of incoherent processors, an argon and helium neon laser were used to illuminate a microscope. The resultant image was so intense that a 1-2 meter diameter image could be projected onto the wall and seen with muted room light. But because the specimen is so small in laser microscopy, speckle was particularly acute and completely destroyed the image. A solution to speckle in coherent imaging of a transparency was demonstrated by Bowman in 1968. [39]. This involved sending the illuminating laser through a rotating wedge of plastic, so the light beam is scanned around in a cone which is then imaged onto the transparency. Each ray of the cone produces the same image but a different speckle pattern, so the speckle is washed out by time averaging as the wedge spins the ray around the cone.

This study uses a more convenient spinning mirror (figure 2.12) to produce speckle free high resolution microscope images. A 1/4-20 bolt goes through a nut that is epoxied to the flywheel for balancing.

Figure 2.13 shows the laser reflected onto the center of the rotating mirror. This mirror is angled so that the beam reflects off at different angles depending on the rotation of the mirror. The condensing lens images the laser spot on the mirror onto the microscope slide and objective. This produces the same effect as with Bowman's prism, but is much easier to implement.

Using an oil immersion lens with a 1.25 numerical aperture (N.A.), the speckle of the argon laser made the image completely unrecognizable, but as soon as the mirror was spun, a speckle free image appeared. The image was nearly perfect except for a small loop of light arising from reflections off the front and back of the

condensing lens. Anti-reflection coatings would remove this noise. This setup produced intense high contrast images of stained nuclei with 514 nm light and stained bacterias with 633 nm light. The 633 nm light was useful for not detecting red blood cells. A fly's wing magnified by this method is shown in figure 2.14.

2.312) Arc Lamp Microscope

The microscope images made with xenon and mercury arc lamps were not as bright as the laser's, but they were in color, and they were much more convenient and cheaper to produce than the laser's. Xenon's color is surprisingly uniform over the visible spectrum, and mercury is concentrated in 4 main lines. Some bacteria images taken with the mercury arc are shown in figure 2.15. The eyepiece used was not made for flat field, so only the center is focussed. The long exposure of the color photograph masks the dimness of the original image. This dimness would probably make the arc lamp microscope useful only for high efficiency holographic correlators.

Figure 2.12 Front and side view of spinning mirror.

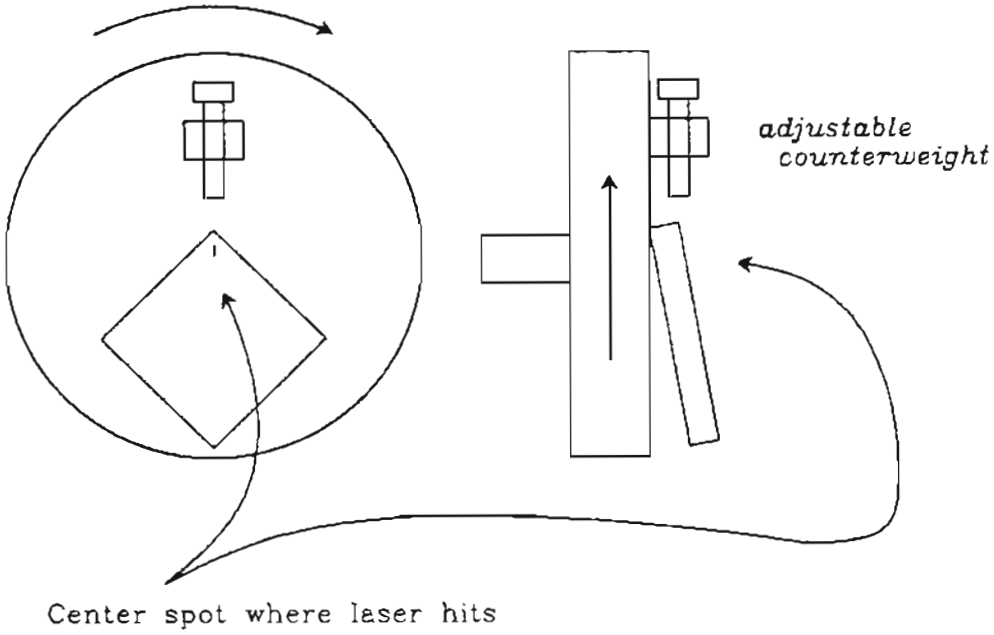

Figure 2.13 Speckle-free laser microscope.

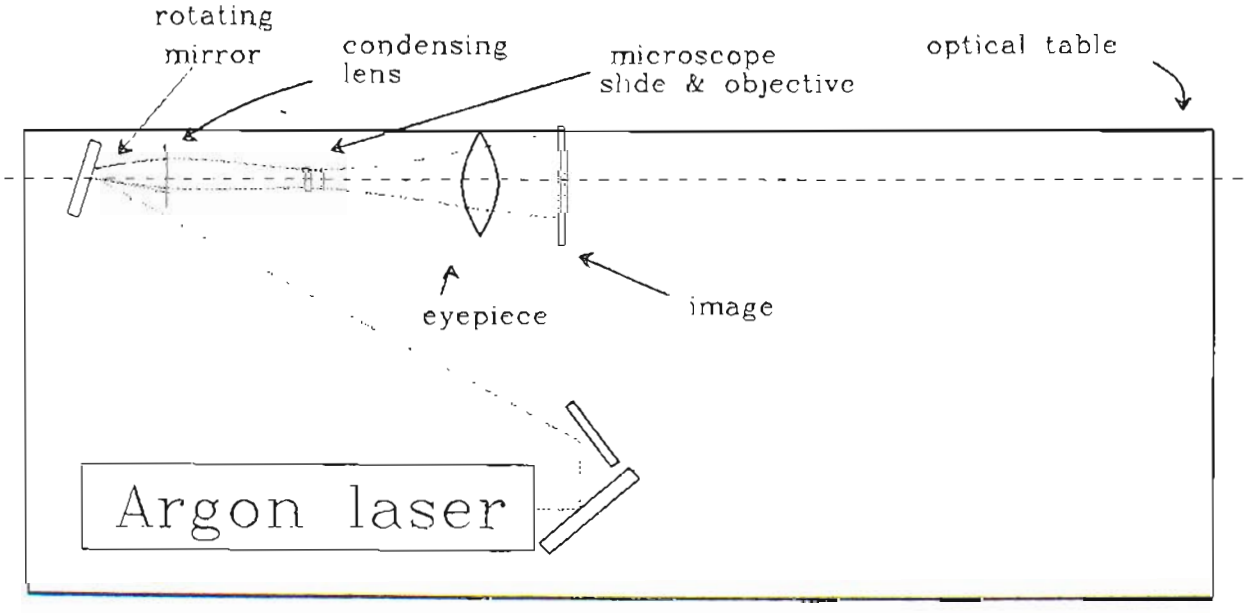

Figure 2.14 Laser microscope's speckle-free image of a fly's wing.

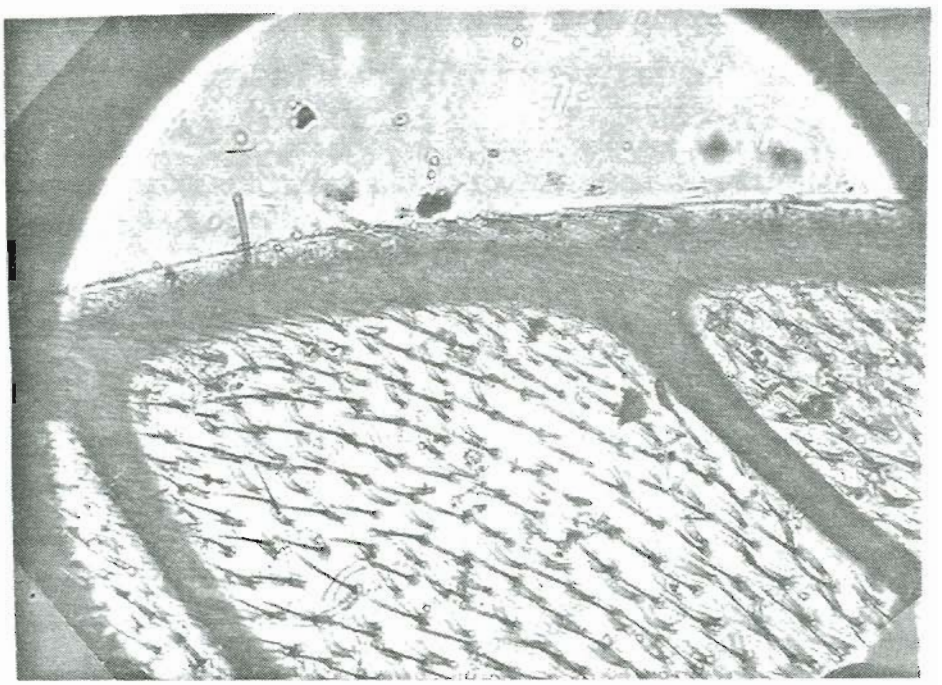

Figure 2.15 Mercury arc lamp microscope's image of bacteria.

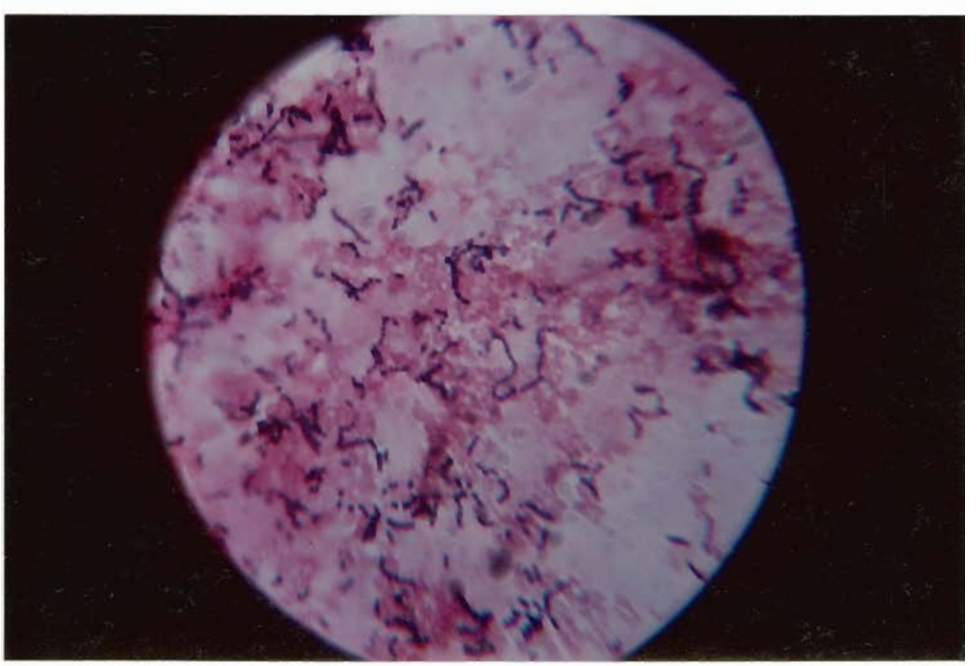

2.32) Preparing Templates

Since it proved difficult to control the amount of bias left in the image with optical edge enhancements, it is lucky that the high contrast photos that are clear where the object is and opaque elsewhere have a low bias to start with. Use of such a negative template to lower the correlation bias was first suggested by Armstrong in his recognition of black and white EEG printouts. This thesis demonstrated that such a technique for producing low bias templates could be generalized for color selectivity by exposing samples of the object to be identified with light of a color strongly absorbed by the object, as was done in chapter 1 with the nuclei. This provided an "opaque-if-not-object to be recognized" template necessary for low correlation bias.

Templates of streptococci bacteria [40] were generated by this method at a 1/2 scale from an original color slide. A 5X negative of this template is shown in figure 2.16.

The author also used a computer graphic editor (GREMLIN) to generate a template of the same bacteria, but the result was so poor in its similarity to the bacteria that it was never used. A negative of it is shown in figure 2.17 only because of the importance of the computer generated technique. Note what good packing density and rotational sampling it provides.

The photographically generated template of figure 2.16 will now be used in a geometrical incoherent optical correlator.

Figure 2.16 Negative of bacteria template photographed from an actual microscope slide.

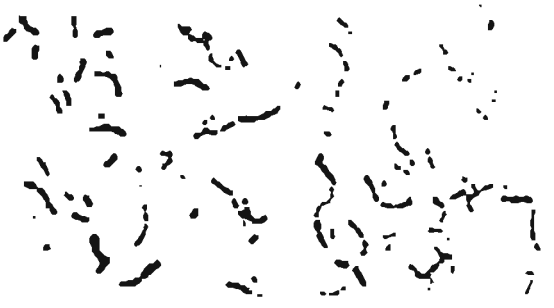

Figure 2.17 Negative of bacteria template made with a computer graphic editor.

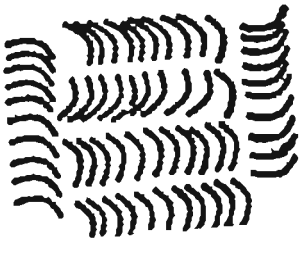

2.33) Correlations with bias

An iris in front of a modified slide projector provided light to a ground glass diffuser. The 35mm color slide of the input scene was placed against this diffuser. Three inches away was the template, and three more inches away was the film or video correlation detector. These two distances were equal because the template was half the size of the original bacteria images. There was no lens used: the correlation was of the geometrical type shown in figure 2.1.

Optical correlations between input scenes and the bacteria template can be seen in figures 2.18,2.19,2.20. The input scene is correlated about the pinhole camera dot in the lower middle of the template. The inputs to the first two are bacteria. As expected, they correlate well with parts of the template that match their shape. The white region is the bias added from the open input aperture. Correlation peaks cannot be detected by blindly thresholding, because the open input contributes a bias which dominates the bacteria's correlation signal.

Figure 2.18-2.20 Correlations with bias

Figure 2.18 Note the indicated pinhole camera scene of 5 bacteria bodies attached together like a bent letter A. This image is convolved onto every point of the template.

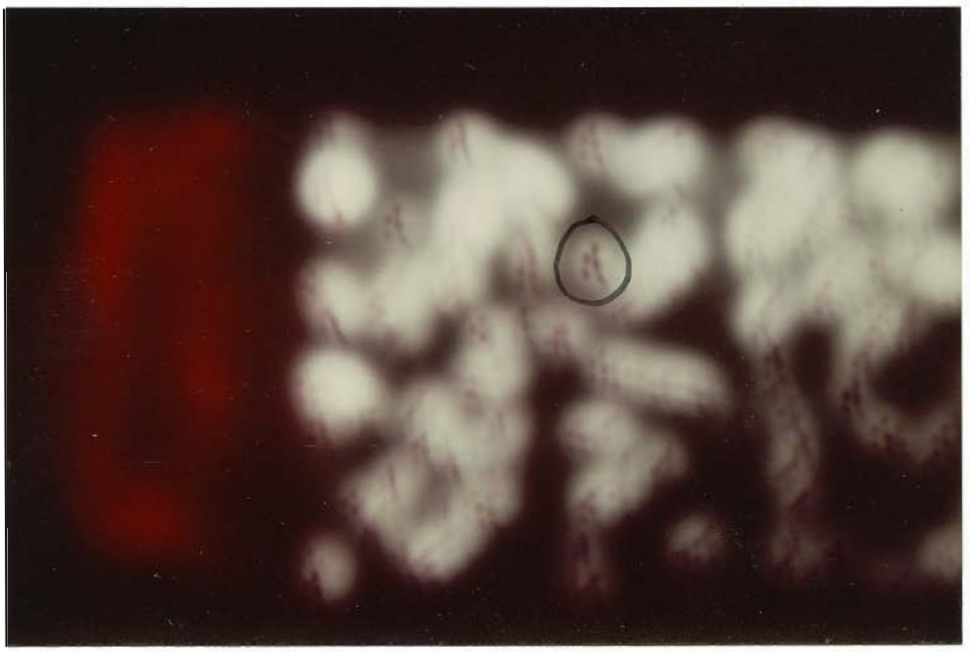

Figure 2.19 Correlation with a bacteria string cupped to the lower left for input.

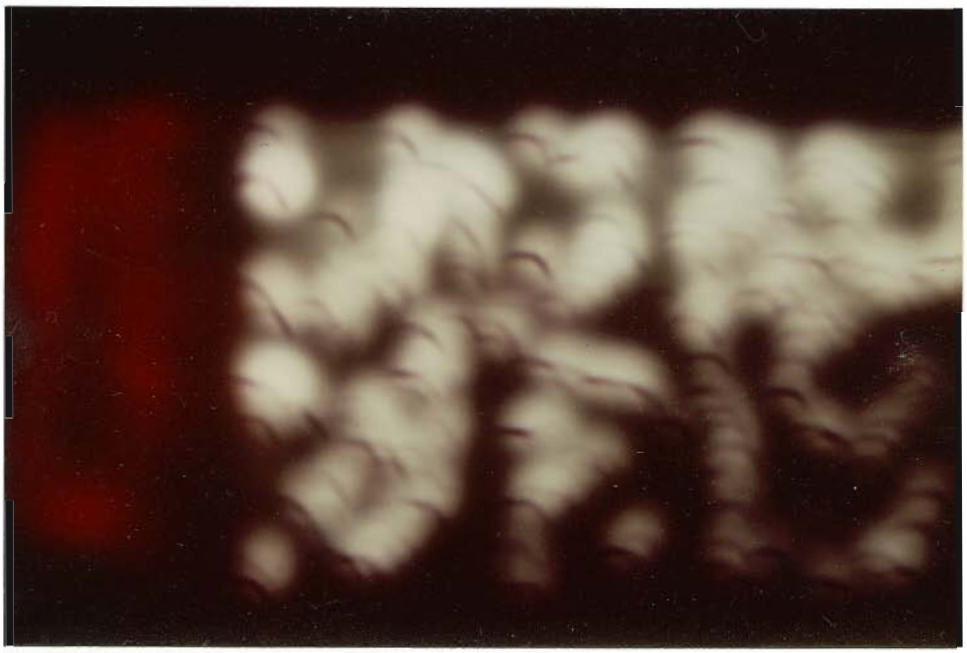

Figure 2.20 Correlation with a collapsed red blood sack for input.

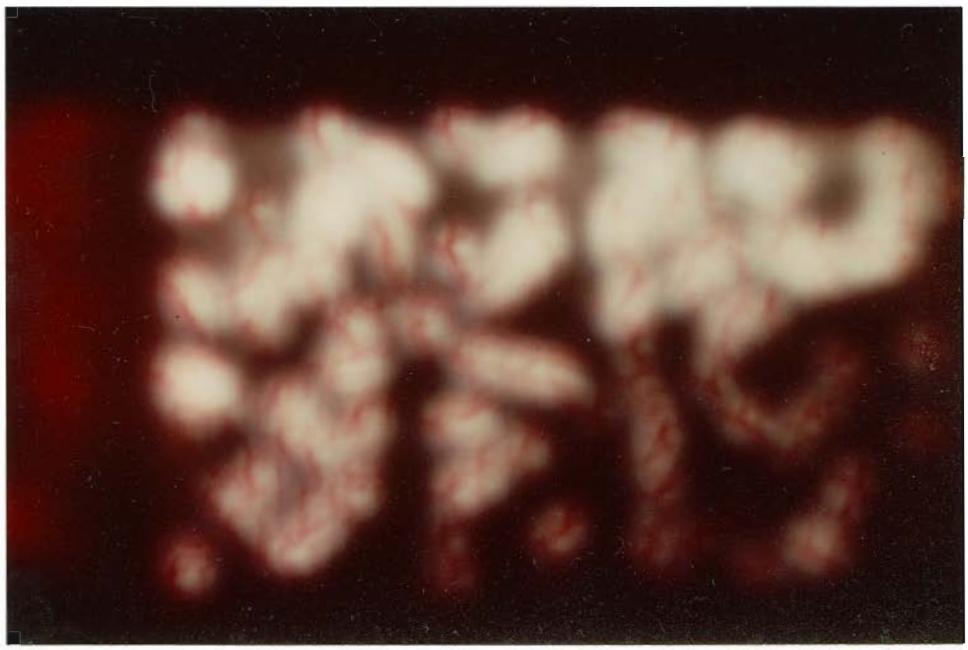

2.34) Lowering the Bias of Inputs

Special application microscope techniques such as dark field [38], phase contrast [38], crossed polaroids, and fluorescence can provide a low background intensity bias in the input. Dark field is the easiest; here only light scattered off the sides of the object is seen, but small objects, like bacteria, only look like points of light. Phase contrast is commonly used because of its ability to examine unstained samples, but it greatly increases the cost of the microscope. Crossed polarizers would work for samples which rotate light's polarization sufficiently, but the natural optical rotation of bacteria is probably too small for any significant image contrast. Fluorescence is one of the best techniques because of the versatility of antibodies and stains. The brightness of the image and the total loss of background bias by use of an interference filter makes fluorescence even more attractive.

2.35) Subtracting Out the Bias

Video frame grabbers can be used to digitize a television camera's signal for a computer. Two images can then be subtracted in the computer. It will now be shown that this allows the removal of the bias.

The distribution of addition over correlation can be easily proven.

$$\begin{aligned} image * template = (a+s)*t &= \int (a(x)+s(x))t(x+k)dx \\ &= \int a(x)t(x+k)dx + \int s(x)t(x+k)dx \\ &= a*t + s*t \end{aligned}$$

The input can be broken into two parts, the aperture (a) and the signal (s). The bias correlation of the aperture and the template (a*t) can be stored once and subtracted point-for-point from each biased correlation to yield the signal correlated with the template with no bias (s*t).

This is similar to work done by Kelly [41] where negative portions of a bipolar impulse response were generated using the Herschel photographic effect. This is an effect, discussed by Kelly, in which film can be darkened normally by blue light, but also lightened with exposure to yellow light. The positive portions of the impulse response were darkened by exposure to UV light, and the negative ones by exposure to a great deal of yellow light. We finally obtained samples of this type of film (AC4 autopositive) from Kodak, but it was much too slow for the low light throughput of the incoherent system, and the UV needed to darken it was absorbed by all the dyes in a color transparency. A more successful technique involved video subtraction.

2.351) Digital Subtraction With Video Camera

Video image subtraction can be performed at real-time rates. The same digital video camera can also perform peak detection. Such a system replaced the SLR

camera used in the incoherent system previously described. An Ikegami ITC-52 video camera and a "Robot" frame grabber [42] were connected to an apple computer running an image subtraction and thresholding program. [43] This system without the microscope would cost five or six thousand dollars.

First the correlation of the empty aperture and the template (a*t) was recorded. The correlation with the inputs of bacteria (a+s)*t and of blood (a+n)*t were recorded, and subsequently had the a*t scene subtracted from them to yield the bias-free input correlated with the template. In practice the subtraction was reversed: a*t - (a+s)*t = -(s*t) causing the previous dark detection "stake" to become light detection "spike". The printing process reversed this light-dark polarity again. The template itself was usually also recorded by putting a pinhole in the input and projecting a shadowgram of the template onto the video camera's photosensor. This is as shown in figure 2.2.

2.352) Color Filtering

A red filter in front of the video camera greatly reduces response to red blood cells and enhances bacteria detection. It was not used however, so that the spatial correlation alone could be examined. Our video camera was equally sensitive to the blue of bacteria and the red of blood cells, so the white light of the slide projector was all that was used.

2.36) Experiment

The previous setup was used with a video camera (template put where the lens is normally). Three sets of images were recorded. The first five (figures 2.21-2.25) show the input, template, correlation with bias, the correlation with the (a*t) bias subtracted out, and a thresholded version of the previous, bias free correlation. The next four figures (2.26-2.29) show the second template and its no-bias correlation with bacteria and circular blood cell sacks. The last photographs of each group (figures 2.25 and 2.29), are of figures 2.24 and 2.27 thresholded at greylevels 10 and 8, with the darkest possible level being 64. In figure 2.25 only the portions of the template parallel to the input bacteria strand have a good enough correlation to be darker than level 10. Figure 2.29 was thresholded at a level (8) which completely excluded any of the red blood cell correlation (figure 2.28).

2.4) Discussion

After discussing figures 2.21-2.29, the two problems still remaining before incoherent optical information processing can achieve its potential will be discussed. These are: 1) normalization of the input and template signals, and 2) peak detection of the correlation. After these are discussed, computer generated templates and input/output devices are examined. The holographic and geometrical techniques of incoherent optical information processing are then compared. Finally, three possible microscope image analyzing products are discussed.

Figure 2.21 is the original signal input of the tilted bacteria strand. Its diagonal line is nearly removed from the linear portion (into saturation) of the grey scale by the dark, circular aperture bias.

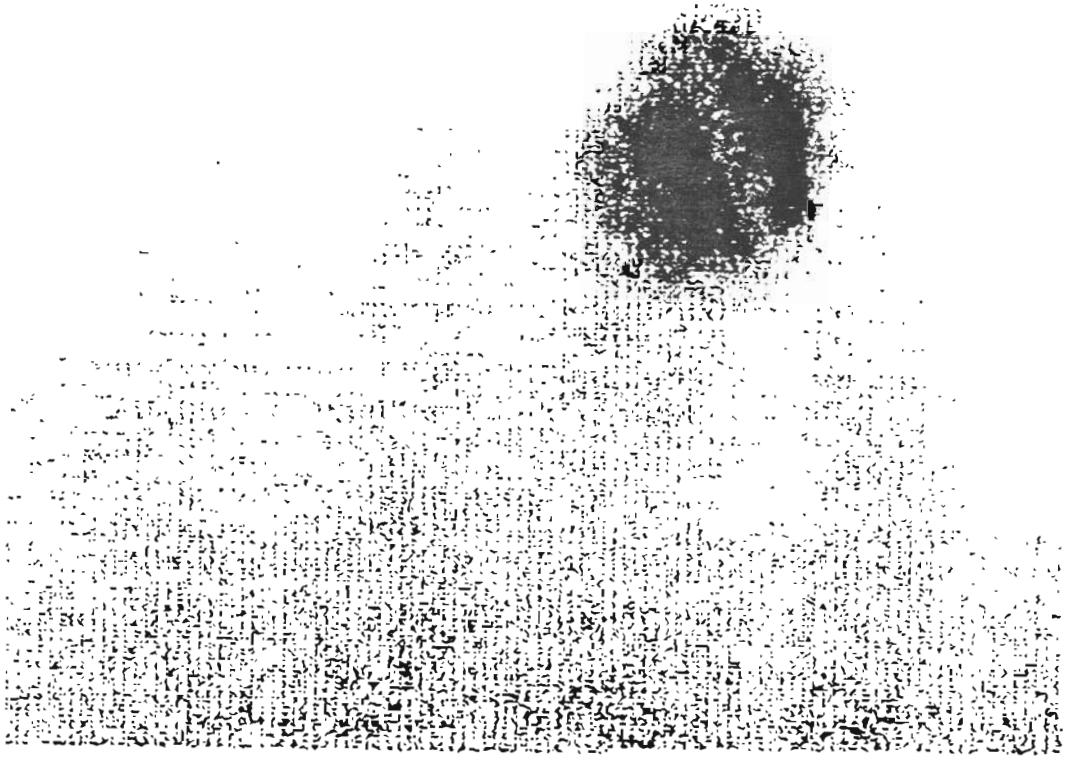

Figure 2.22 is the template projected with a point source as in figure 2.2. The individual circles are individual bacteria (circular=cocci), and their groupings are characteristic of their type (strep). The limited space-bandwidth of video only allows a few colonies to be recorded on the template.

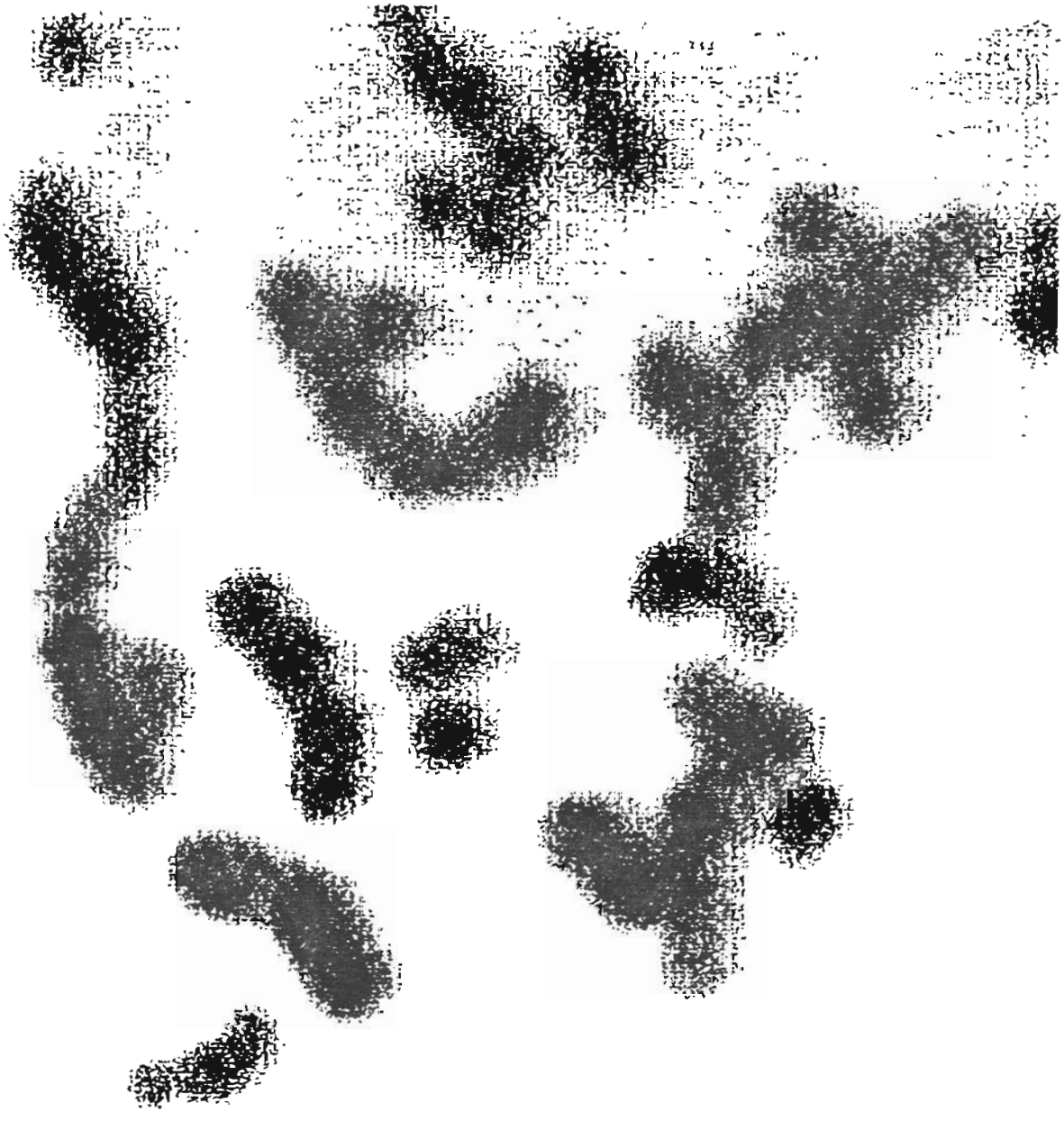

Figure 2.23 is the full (aperture+ signal) input correlated with the template. The correlation of the signal with the template can barely be seen as light, diagonal lines in the areas where the template's bacteria were tilted at the same angle as the input. The larger dark areas are from the correlation of the empty aperture and the template, and this bias obscures the bacteria's correlation.

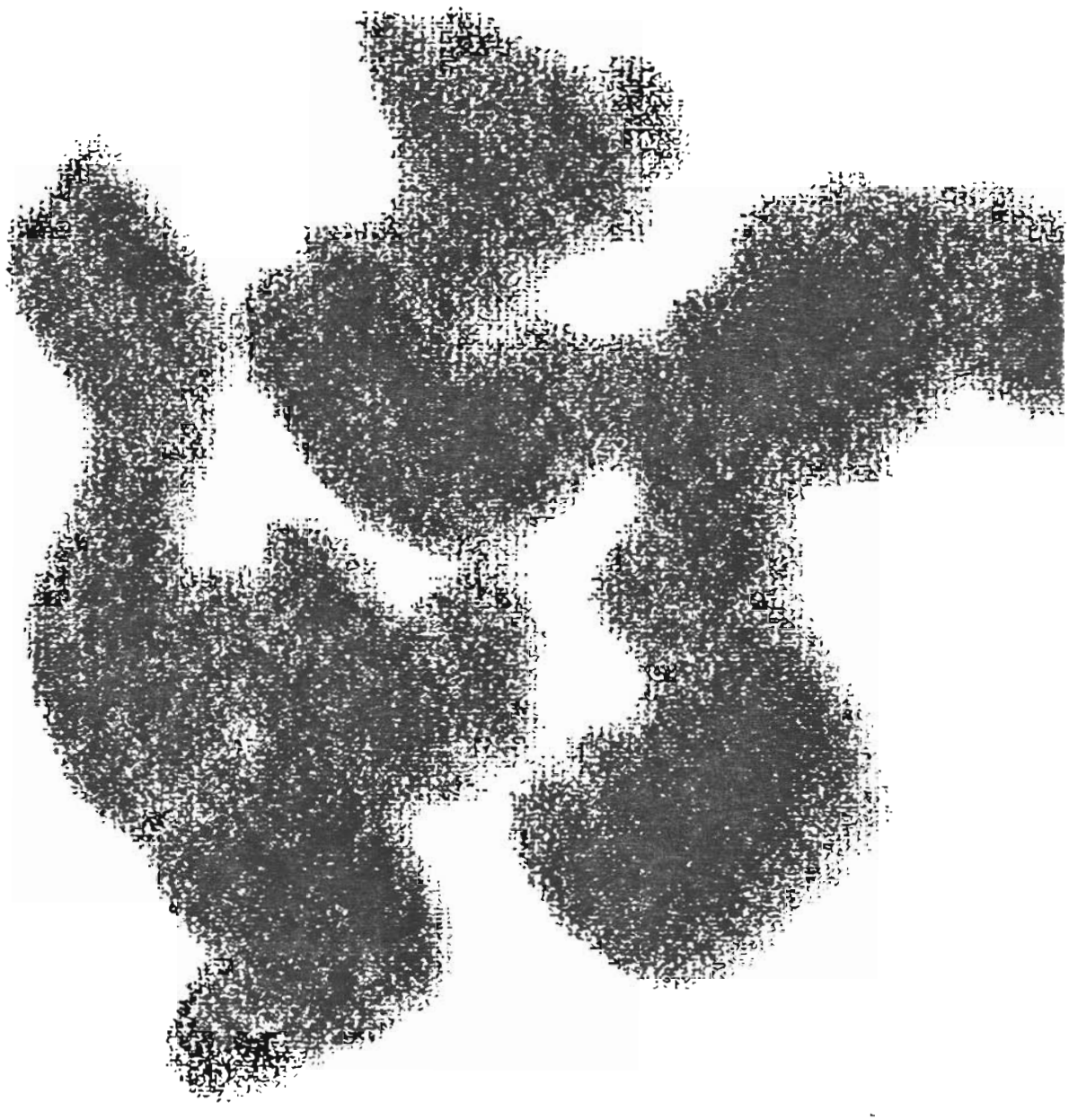

Figure 2.24 is the signal-correlated-with-the-template, and it is produced by subtracting off the aperture-correlated-with-the-template from the biased correlation of figure 2.23. The large, dark bias areas have been removed from the image, showing only the desired correlation. Inside the circled area are both good and poor correlations. Where the template is tilted at the same angle as the input signal, there is a concentration of darkness. To the lower right, where the template is perpendicular, the poorer correlation is more spread out.

Figure 2.25 is a thresholded image of the previous figure 2.24. Any grey value under 10 (out of 63) was cancelled with a zero at that spot. Grey values greater (darker) than the threshold of ten are passed unchanged. Only those parts of the correlation which correspond to the template being oriented at the same angle as the input have darker values than ten.

Figure 2.26 Second bacteria template.

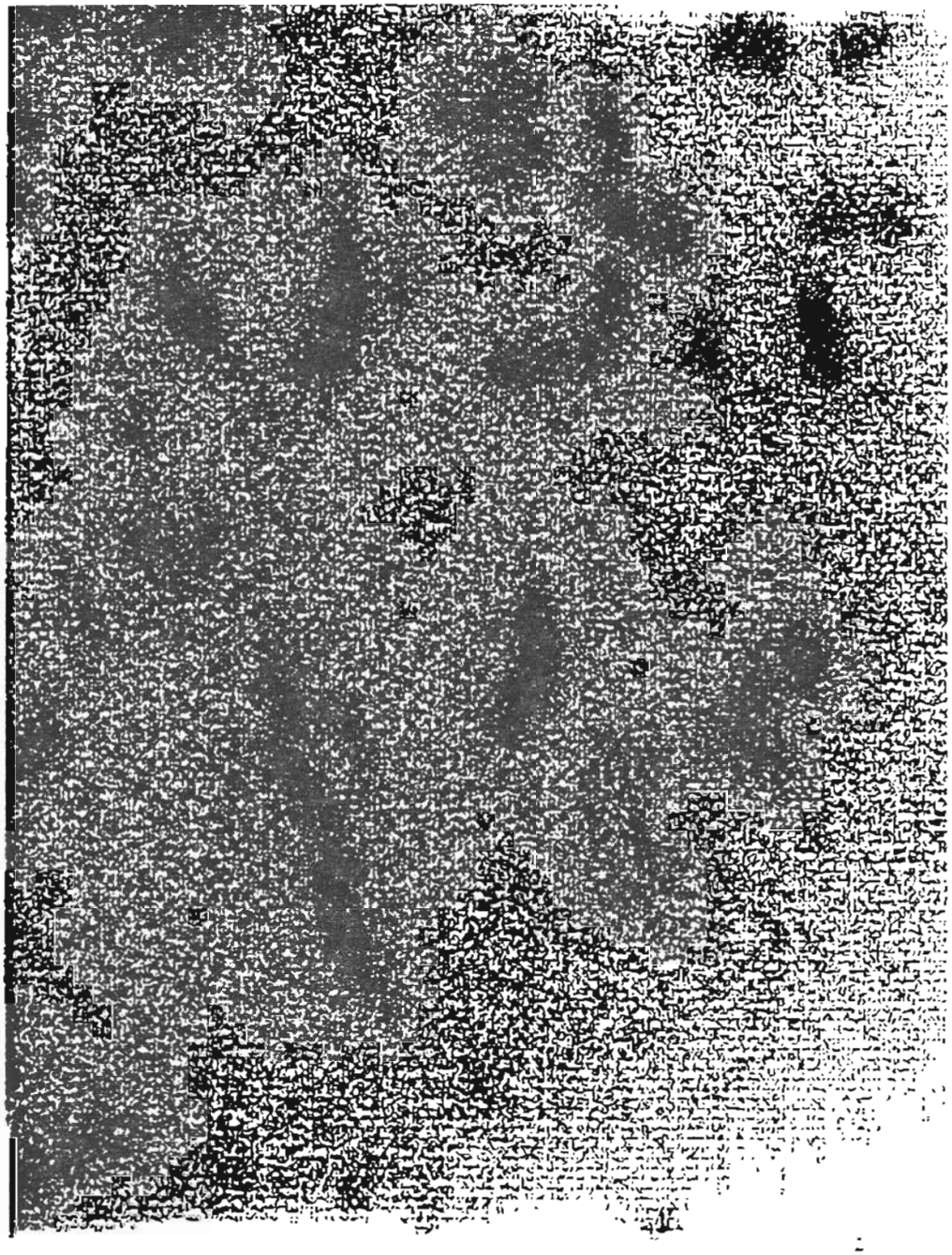

Figure 2.27 is the second template (figure 2.26) correlated (*) with a vertical bacteria input. The darkness is concentrated where the template images were vertical.

Figure 2.28 is the template correlated (*) with a round red blood cell. Nowhere is the darkness as concentrated as in the more similar bacteria template shown in the previous figure.

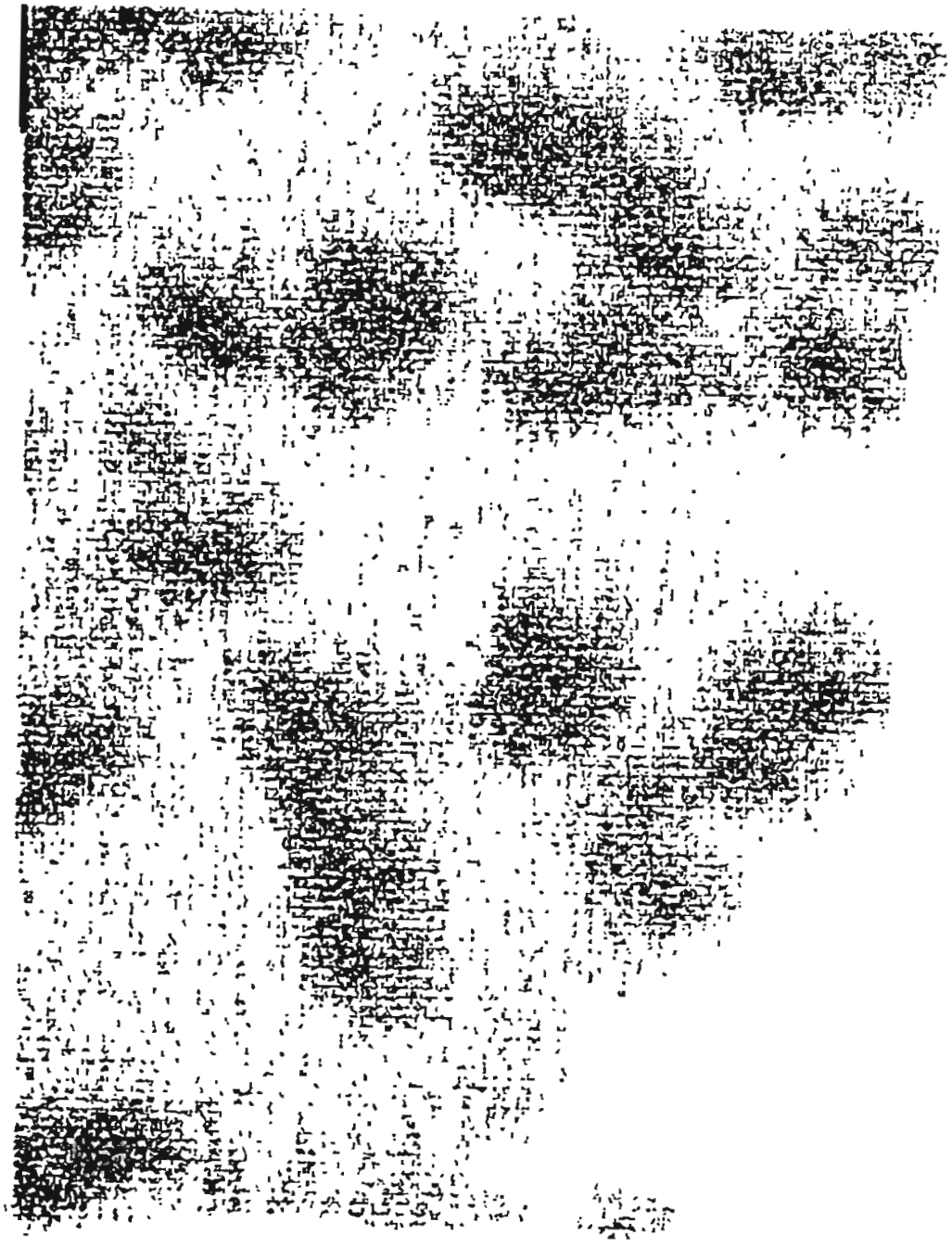

Figure 2.29 is the previous figure 2.27 thresholded at grey value 8 out of 63. The same orientation selectivity is shown here as in figure 2.25. No points of figure 2.28, the correlation with the blood cell, are darker than 8, so a photograph of this correlation would be a wasted blank. This illustrates how successfully this system can locate bacteria in blood even without color selectivity.

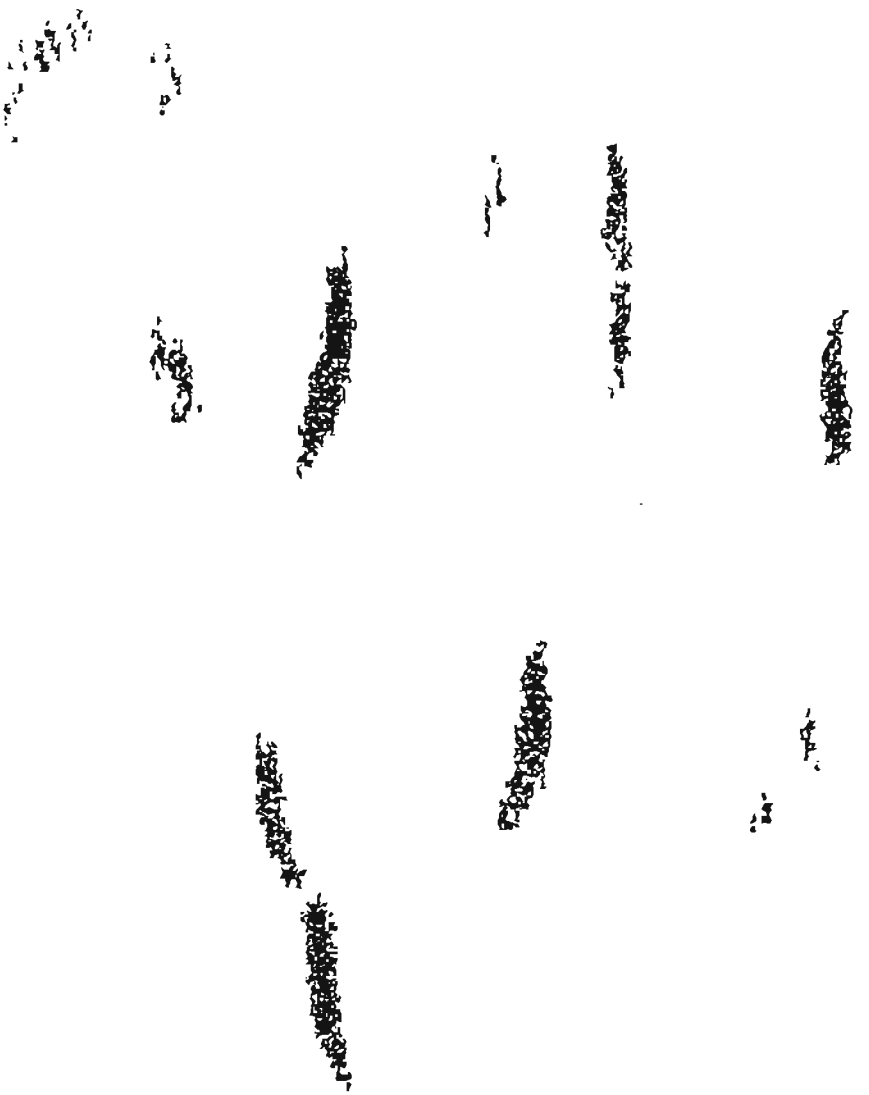

2.41) Normalization

It is useful to treat images as vectors in a function space defined over a two dimensional, continuous, real domain (x,y). Using this notation, we start with correlation of the input i and template t:

$$\hat{\imath} * \hat{t} = i\hat{\imath} * t\hat{t} = it(\hat{\imath} * \hat{t})$$

It is the correlation with the unit vectors $\hat{\imath}$ and $\hat{t}$ that interests us. The scalars i and t, representing the relative intensity or transmittance of the input or template, need to be "normalized" out. This can be done easily for t by making all the template images have the same total "energy":

$$\int t(x,y)dxdy = a\ constant \text{ for } all\ images \text{ if and } only \text{ if } \hat{t} = \hat{t}$$

It is more difficult for $\hat{\imath}$, the input image, since its unknown nature requires feedback during or after the measurement. If $\bar{a}=0$ (no bias) then the illumination can be controlled to keep $\int \hat{\imath}$ = (the total image energy) constant, as is done in the fluorescent urine analyzer to be discussed. If $\bar{a} \neq 0$, then such feedback would also vary $\int \bar{a}$ = (*the energy the empty aperture*), so that a different bias correlation $(\bar{a} * \hat{t})$ would have to be subtracted out by the frame grabber. Unfortunately, big or small input intensity values would go into non-linear ranges of the image detector, which records a finite number of grey levels. The frame grabber we used recorded 64 grey levels.

2.42) Peak Detection

Autocorrelation will always provide a higher peak value than cross-correlation: $\max(f*f) \geq \max(f*g)$. The detection of this peak is the major bottleneck in optical information processing. In this study it was done by computer after video detection, so the camera must sample many points of each correlation to detect a peak. This restricts the correlator to the low space-bandwidth-frequency product (SBF) of the video system which, in this thesis, produced poor resolution correlations with tens of template sub-images. There is no reason to go to the higher information densities of the holographic templates as long as this video bottleneck exists.

In order to use the extremely high SBF products of holographic correlators, a nonlinear, analog peak detection technique is required. The nonlinearity would cause those archetypes with high correlation peaks to produce more total light. Then, each pixel of the video detector could examine whether there was a good correlation with a single archetype. A 512 X 512 detector could examine the input correlated with $(512)^2 = 262{,}144$ high resolution micro-images for the analog correlation process.

Possible candidates for this important analog peak detection are: fluorescence, optical bleaching, second harmonic generation (SHG), and optical bistability. Fluorescence is unfortunately linear. Optical bleaching and SHG require much too high powers. Optical bistability is an active area of research and hopefully will provide a solution. [44]

2.43) Computer Generated Template

Since templates must usually be developed into transparencies or holograms, there is enough time to use a computer to generate the individual images. Each image will be enhanced with those colors and spatial frequencies which make it different from the noise. This accentuation is why the individual template images t_i are called archetypes. The computer will also normalize the individual template images, and pack them closely together.

The hologram can hold so many images that each archetype might be replicated many times on the template, each one rotated or scaled slightly differently.

2.44) Input / Output

Video is certainly the most mature image I/O technology. Real time frame subtractors and thresholders allow the bias to be removed and peaks detected in real-time. [45] CRT phosphors can also be made with narrow color spectra for use as inputs for holographic correlators. [28] The well-known but expensive liquid crystal light valve can be used as a real-time transparency template. However, two new devices show great promise.

The optical RAM [46] uses actual computer memory as the photosensor material. The image is cast through a window on the top of the chip onto the memory. 64k memory is standard now, but the company producing them plans to continue to move up in size as the standard chips do, so there should be one megabyte image chips soon. Unlike normal methods of computer communication

between memory and processor, an image cast onto memory has no input bottleneck. The software interface is just a BASIC PEEK statement. Optical RAMS are as cheap as normal memory chips, and can be memory strobed [47] at different speeds to provide grey levels. That is, to sample for very intense areas, the computer can strobe in rapid succession and not give the individual photosensors of the RAM enough exposure time to increase their voltage sufficiently to turn on. To sample for low intensity areas, the computer strobes the memory in slow succession to give the individual photosensors a long exposure time. Unfortunately, the memory must be strobed at least once a second or the accumulated charge in one pixel leaks into its neighbors. This means that bright room lighting is necessary to obtain an image when the optical RAM is used as a normal camera, making it too insensitive for incoherent optical information processing. Fortunately, military work [48] on image intensification with microchannel plates may solve this problem for optical RAMs.

Liquid crystal television sets for the consumer market can be used as inexpensive light valves. Color liquid crystal television sets are now readily available, and their images are stable enough to record holograms [49].

2.45) Comparison of Holographic and Geometric Correlators

As was shown earlier, both holographic and geometrical systems would allow scaling of the images.

Geometrical templates have poor light throughput, but multi-color templates are easily made with color film. Holographic templates have good light throughput, but color control is more difficult with holograms, involving reflection holograms exposed with a dye laser or multiple transmission holograms, each with its own color selective filter.

Information *densities* are thousands of times higher in holograms, but the low resolution of geometrical templates can be compensated for by enlarging the template until it can hold all of the required archetypes.

2.46) Three Possible Microscope Image Analysis Products Based on IOIP

1) Urine Analyzer for Dysplastic Cell Nuclei

Kidney, bladder, and prostate problems can often be detected by examination of cells found in the urine. To analyze urine, it would be first treated with fluorescent nuclear stain. Excited by a mercury vapor lamp, only the fluorescence would transmit through an interference filter to the detector. Since there is no bias, the input energy can be normalized by a photosensor controlling the mercury lamp's current. A transparent template could be used, or a holographic one if the fluorescense of the stain was narrow enough. The detection would be done by video. This would allow 30 cells/second to be correlated with at least tens of other nuclear images.

2) Bacteria Detector.

Bacteria often need to be detected. Two cases we will deal with here are in blood and drinking water.

The system developed in this thesis for detecting bacteria in blood worked well even though it used only spatial correlation. With the addition of a red filter, the blue bacteria darken the correlation even more, but the red blood cells hardly

register.

Such a bacteria locator is important for hospitals. Even the sickest patients have very few live bacteria in their blood, and the microbiologist would be wasting his time to look for enough bacteria for a diagnosis. [40] Instead, blood is taken from the patient and incubated for 18 hours. This is long enough for the bacteria, free from the body's defenses, to grow numerous enough for the microbiologist to diagnose. This is an unfortunate delay in the beginning of treatment.

It would therefore be useful if an incoherent correlator similar to the one developed in this thesis could be mounted on a microbiologist's microscope to allow it to store the video images which are likely to have bacteria. The microbiologist could then examine these images to make the diagnosis.

Bacteria in drinking water cannot be stained if continuous monitoring of the flow is needed. Phase contrast could provide an image, which would be examined by frame subtraction methods used in this thesis. The correlation value would control the amount of chlorine released.

3) Tissue Analyzer

Because of the small field of view of a microscope, a square inch of tissue represents an unwieldy amount of information. A simple "map" of the tissue, categorizing different areas of the slide, would greatly help the pathologist by ordering the voluminous information. To accomplish this, a standard microscope slide would be moved by a digitally controlled stage to scan the entire slide over the

input. An optical correlator would classify tissue areas of the slide, producing a contour map showing percent correlation with different tissue archetypes. Different templates could be inserted for different organs.

A color video camera would look at the input through a color template. There would be no video frame subtraction, since the whole aperture would be filled with tissue and thus there is no aperture to subtract out. The best that can be done is for the computer to look for correlation information on the expected triangular bias.

Only experiment will tell how well the color and spatial frequency enhanced templates discriminate different tissue states, but they probably would be able to help a computer attempting the same task.

III) CONTRIBUTIONS AND ACHIEVEMENTS OF THIS THESIS

1) In the first chapter the researcher developed theoretical models of the optical diffraction pattern of a photograph of a human cell nucleus to create techniques which rapidly estimated the nucleus' four important descriptors of size, shape, darkness, and texture. These techniques were successfully implemented on optical equipment which the researcher designed and constructed.

2) In Chapter 2, the researcher was the first to apply incoherent optical information processing techniques to pattern recognition of microscopic cell images. This thesis also contains the first explanation of the value of this application.

3) The high resolution and high contrast technique that was invented in Chapter 1 for photographing an entire field of nuclei, led in Chapter 2 to the production of high quality templates for incoherent image correlation.

4) The discovery in Chapter 1 that image information about nuclear size and shape was contained in the medium spatial frequencies and texture information was contained in the higher spatial frequencies led, in Chapter 2, to the idea of spatially bandpassing certain spatial frequencies of the templates to make them more selective to the characteristics of the cells to be detected.

5) The geometrical requirement of equal reference and object angles for proper functioning of holographic correlators was discovered, as were the correlator's scaling properties. High quality holographic templates were made of human nuclei.

6) In order to add color selectivity as well as spatial frequency selectivity, a new method of edge enhancing color slides was developed using spatially coherent

white light. As part of this research a convenient new folded transform setup and new liquid gate were also developed for coherent image processing.

7) Light throughput problems inherent in incoherent optical information processing were examined, and the researcher concluded that dichromated gelatin (DCG) technology would be useful. The researcher then acquired that technology. See appendix G for theory and recipe.

8) The exacting requirements of a classical, high-resolution microscope were achieved using basic components. Then, to get an intense input image, a laser microscope was built, and a convenient spinning tilted mirror technique was invented to remove the speckle noise which plagues laser microscopes.

9) The problem of build-up of the input image bias was solved by noting the linearity of correlation and breaking the input into two parts: aperture and signal, and then subtracting out most of the bias (a*t). Methods of lowering the bias of the input were also discussed.

10) Three possible new commercial medical products using incoherent optical information processing were suggested in detail.

11) Finally, an analog method of peak detection was identified as an essential breakthrough before incoherent optical information processing could achieve its potential.

In summary this researcher independently:

- identified an important area of application,
- obtained assistance from physicians and learned more about their specific needs,

-used a coherent optical technique to approximate the four most important diagnostic clues of human nuclei, but rejected this easier coherent technique because of the poor performance of light valves,

-unified the different kinds of incoherent correlators.

-developed techniques for producing quality templates for incoherent correlators,

-built prototype incoherent correlator systems,

-and used one such system to successfully locate bacteria in blood.

While many of the investigated prototype systems may prove useful eventually, the system used to locate bacteria in blood is ready to be upgraded for automated, real-time clinical use in hospitals..

Conclusion

Present day computers rest on great mathematical achievements in the areas of logic, combinatorics, and algebra. An equally rich mathematical legacy for optical information processing has been provided by quantum mechanics and linear system theory. OIP provides the means for accomplishing inner products. This allows linear transformation or pattern recognition to be accomplished in parallel over gigantic memories at the speed of light. Images are also convenient data types because humans rely so heavily on their eyes, and there is a great deal of technology developed for recording and displaying images.

The hardware potential is staggering: processing *rates* many orders of magnitude larger than what we dream of in *static* memory. However, some technique must be found for analog peak detection, because without it the large space bandwidth frequency (SBF) of optical information processing must pass through a much smaller SBF of video peak detection.

Appendix G: Dichromated Gelatin

Gelatin is made by dissolving collagen in hot acid or base. The structural protein collagen makes up 90 percent of a mammal's protein. Each collagen molecule is a triple helix of protein chains. Like most proteins, gelatin has a COOH group on one end and a NH2 group on the other. The COOH looses a proton in a basic solution, and the NH2 gains a proton in an acidic solution. These ions, spread throughout the gelatin, repel each other. This causes very large swelling at ph values far from the isoelectric ph of 4.5 .

Hardening = crosslinking of gelatin = less swelling & higher melting point. The process of "hardening" or "tanning" of gelatin or collagen is ancient. Indeed, tanned collagen was our first plastic. Some leather processes hardened the collagen with Cr.+3 ions (usually as Chromium Potassium Sulphate). It was also known that the Cr+3 could be produced by blue light hitting dichromate Cr +6 ions. Talbot began using this effect as a resist in the mid 1800s, and many high resolution photoresists were made by varying the solubility of soft gelatin. Holograms are recorded when light reduces dichromate ions in the gelatin to triply charged chromium atoms which crosslink COOH groups of the gelatin.

Felt Model

When put in water, the gelatin is constrained from swelling by the crosslinks formed by the exposure of the periodic interference pattern. The gelatin molecules connected by these crosslinks can be viewed as a spaghetti held together by many small springs which stretch and break as the gelatin swells. Swelling and solubility can be increased by higher temperatures or by extreme ph values. Soft gelatin can

be dissolved or pulled toward the harder regions. In a fully swelled "developed" gelatin "felt" the mass density, which is proportional to the index of refraction, is now roughly proportional to the original periodic exposure intensity. The gel is dried in increasing alcohol/water concentrations of increasing temperature to keep the felt of gelatin from collapsing. Exposing the dried hologram to humidities > 85 percent will swell and destroy the image. Applying pressure to the gelatin will cause the periodic layers to collapse and destroy the image.

The thickness of the emulsion can be controlled, along with the reconstruction wavelength and bandwidth. DCG holograms can be as nearly noise-free as a glass plate and have diffraction efficiencies in the 50-100 percent range. When properly sealed they will probably last forever.

Dichromated Gelatin Experimental Technique

Several experimental procedures for coating, developing, and exposing were tried. This one was found to produce the best results. It is similar to other recipes. [34]

1) 7 percent gelatin

2 percent Ammonium Dichromate (very dangerous oxidizer!)

coated onto 2"x3" microscope slides with a modified doctor blade consisting of a steel spring which has a 1/4" steel rod going through it. The blade was swept across the gelatin in about 2 seconds.

2) Dried horizontally

3) Expose 30 mj/sq.cm at 488nm.

4) Develop

a) Rapid fix with hardener 10 sec.- 2 min. In the first 10 seconds the hypo in the fixer reduces the residual dichromate, hardening the gelatin and removing the yellow stain. The fixer is also buffered by Boric acid to ph=4.5, ensuring the initially soft gelatin doesn't swell apart.

b) Wash in water 2 min. (68-90 degree F.)

Higher temperature swells the emulsion more, producing a brighter image but with more scattered noise.

c) Dehydrate

1) 70 percent water / 30 percent isopropanol

2) 70 percent isopropanol/ 30 percent water

3) 100 percent isopropanol

4) Dry quickly with hot air gun.

5) To seal properly, 3/8" edges must be scraped free of gelatin and a glass plate glued on

References

1. Bragg, *Nature 154,69 (1944).*
2. *Applied Optics and Optical Engineering III,* p. 159, Academic Press, 1965.
3. *The New FACS 400 Series Fluorescence Activated Cell Sorting,* Becton Dickinson (408)-738-8558.
4. J. Leger, *Applications of Optical Fourier Transforms,* p. 153, Academic Press, 1982.
5. F. Paul Carlson, *Introduction to Applied Optics for Engineers,* Academic Press, 1977.
6. B. Pernick, R.E. Kopp, J. Lisa, J. Mendelsohn, H. Stone, and R. Wohlers, "Screening of Cervical Cytological Samples Using Coherent Optical Processing," *Applied Optics,* pp. 21-51, January 1, 1978, Vol.17, No.1.
7. Bernhard Turke, Gunter Seger, Manfred Achatz, and Werner V. Seelen, "Fourier Optical Approach to the Extraction of Morphological Parameters from the Diffraction Pattern of Biological Cells," *Applied Optics,* pp. 2754-2761, Sept. 1, 1978.
8. *Hughes Aircraft makes these light valves.*
9. Charles P. Miles,M.D. and Dwight L. Jaggard, Ph.D., "The Use of Optical Fourier Transforms to Diagnose Pleomorphism, Size, and Chromatin Clumping in Nuclear Models," *Analytical and Quantitative Cytology Journal,* pp. 149-155, Vol. 3 No.2, June 1981.
10. John S. Carrol, *Photographic Facts and Formulas,* p. 132, Prentice-Hall, 1976.
11. Siegman, *Introduction to Lasers and Masers,* p. 316, McGraw-Hill, 1971.
12. Taylor and Lipson, *Optical Transforms,* p. 91, Cornell Univ. Press, 1964.
13. *A liquid gate must be used in all coherent optical processing, because the diffuseness of photographic film's surface must be cancelled by immersion into an index matching fluid such as xylene held between two optically flat windows.*
14. W.Vaughan, "Dove Prisms-Properties and Problems," *Optical Spectra,* p. 68, October,1981.
15. J.W.Goodman, *Introduction to Fourier Optics,* p. 65, McGraw-Hill, 1968.
16. G.L.Rogers, *Noncoherent Optical Processing,* Wiley, New York , 1977.
17. William T. Rhodes, "Incoherent Spatial Filtering," *Optical Engineering* , p. 323, May-June 1980.
18. M.A. Monahan, K. Bromley, and R.P. Bocker, "Incoherent Optical Correlators," *Proceedings of the IEEE, vol.65, no. 1,* p. 121, January 1977.
19. J.Knopp and M.Becher, "Generalized Model for Noncoherent Optical Convolvers and Correlators," *Applied Optics,* p. 984, April 1978.
20. P.Jackson, "Correlation Function Spatial Filtering with Incoherent Light," *Applied Optics* , p. 1272, July 1967.
21. Eugene L.Green, "Diffraction in Lensless Correlation," *Applied Optics vol.7,no.6,* p. 1237, June 1968.

22. A.W. Lohman, "Matched Filtering with Self-Luminous Objects," *Applied Optics*, p. 561, March 1968, vol.7, no.3.

23. B.J. Thompson, *Coherent Optics,* p. 9, Univ. of Rochester Institute of Optics Short Course Study Guide.

24. S.Benton, *Handbook of Optical Holography,* Chapter on photographic handling., Academic Press, 1979.

25. A.W. Lohman and H.W. Werlich, "Incoherent Matched Filtering With Fourier Holograms," *Applied Optics*, pp. 670-672, March 1971.

26. R.J. Bieringer, "Optical Correlation Using Diffuse Objects," *Applied Optics*, pp. 249-254, February 1973.

27. W.T. Maloney, "Lensless Holographic Recognition of Spatially Incoherent Patterns in Real Time," *Applied Optics*, pp. 2127-2131, September 1971.

28. W.T. Maloney, "Real-Time Holographic Filtering of Oscilloscope Traces," *Applied Optics*, pp. 2554-2555, November, 1971.

29. P.R. Armstrong and A.P. Anderson, "Direct Matched-Filtering of Pen Recordiugs Using Sodium Light," *Applied Optics*, pp. 2337-2339, October 1975.

30. Rand C. Sherman, Grieser, Gamble, Verber, and Dolash, "Hybrid Incoherent Optical Patern Recognition System," *Applied Optics*, pp. 3579-3582, November 15,1983.

31. S. Benton, "The Mathematical Optics of White-Light Transmission Holograms," *Proceedings of the International Symposium on Display Holography*, July 1982.

32. W.S.Colburn, "Holographic Optical Elements," *Air Force Avionics Lab Report TR-72-409*, October 1972.

33. R.T. Ingwall, "Hologram Recording With a New Polaroid Photopolymer System," *SPIE 523*, p. 306, Jan.1985.

34. R.Schlesinger and F. Unterseher, *Dichromated Gelatin Holograms:A Reliable Method,* p. 79 , Lake Forest College Proceedings of the 1982 International Symposium on Display Holography., 1982.

35. M. Wohlers, "Optical Matched Filtering of Incoherent Images," *Applied Optics*, pp. 3584-3550, November 1, 1979.

36. R.Voss and D. Thomsen, "Making Music- Fractally," *Science News*, p. 187, March 1980.

37. D.Casasent and et al, "Application of the Liquid Crystal Light Valve to Real-Time Optical Data Processing," *Optical Engineering*, p. 371, July/August 1978.

38. R. Kingslake, *Optical System Design,* p. 198, Academic Press.

39. Malcolm J. Bowman, "Two New Methods of Improving Optical Image Quality," *Applied Optics Vol.7, no.11*, p. 2280, Nov. 1968.

40. *Dr. A. Rashad is director of clinical microbiology at the University of Oregon Health Sciences Center. I am grateful for his supplying the bacteria images.*

22. A.W. Lohman, "Matched Filtering with Self-Luminous Objects," *Applied Optics*, p. 561, March 1968, vol.7, no.3.

23. B.J. Thompson, *Coherent Optics,* p. 9, Univ. of Rochester Institute of Optics Short Course Study Guide.

24. S.Benton, *Handbook of Optical Holography,* Chapter on photographic handling., Academic Press, 1979.

25. A.W. Lohman and H.W. Werlich, "Incoherent Matched Filtering With Fourier Holograms," *Applied Optics*, pp. 670-672, March 1971.

26. R.J. Bieringer, "Optical Correlation Using Diffuse Objects," *Applied Optics*, pp. 249-254, February 1973.

27. W.T. Maloney, "Lensless Holographic Recognition of Spatially Incoherent Patterns in Real Time," *Applied Optics*, pp. 2127-2131, September 1971.

28. W.T. Maloney, "Real-Time Holographic Filtering of Oscilloscope Traces," *Applied Optics*, pp. 2554-2555, November, 1971.

29. P.R. Armstrong and A.P. Anderson, "Direct Matched-Filtering of Pen Recordings Using Sodium Light," *Applied Optics*, pp. 2337-2339, October 1975.

30. Rand C. Sherman, Grieser, Gamble, Verber, and Dolash, "Hybrid Incoherent Optical Patern Recognition System," *Applied Optics*, pp. 3579-3582, November 15,1983.

31. S. Benton, "The Mathematical Optics of White-Light Transmission Holograms," *Proceedings of the International Symposium on Display Holography*, July 1982.

32. W.S.Colburn, "Holographic Optical Elements," *Air Force Avionics Lab Report TR-72-409,* October 1972.

33. R.T. Ingwall, "Hologram Recording With a New Polaroid Photopolymer System," *SPIE 523*, p. 306, Jan.1985.

34. R.Schlesinger and F. Unterseher, *Dichromated Gelatin Holograms:A Reliable Method,* p. 79 , Lake Forest College Proceedings of the 1982 International Symposium on Display Holography., 1982.

35. M. Wohlers, "Optical Matched Filtering of Incoherent Images," *Applied Optics*, pp. 3584-3550, November 1, 1979.

36. R.Voss and D. Thomsen, "Making Music- Fractally," *Science News*, p. 187, March 1980.

37. D.Casasent and et al, "Application of the Liquid Crystal Light Valve to Real-Time Optical Data Processing," *Optical Engineering*, p. 371, July/August 1978.

38. R. Kingslake, *Optical System Design,* p. 198, Academic Press.

39. Malcolm J. Bowman, "Two New Methods of Improving Optical Image Quality," *Applied Optics Vol.7, no.11*, p. 2280, Nov. 1968.

40. *Dr. A. Rashad is director of clinical microbiology at the University of Oregon Health Sciences Center. I am grateful for his supplying the bacteria images.*

41. D.H.Kelly, "Image Processing Experiments," *Journal of the Optical Society of America* , p. 1095, 1961.
42. *This video equipment was supplied by Drs. Elliott and DeFreez.*
43. *This software was written by Bob Cary of Sunset Labs.*
44. "Optical Bistability : Where is it headed?," *Laser Focus* , October 1985.
45. *Colorado Video sells such a real-time device.*
46. Micron Eye, *Micron Technologies, Inc*, Boise, Idaho 208 386 3800.
47. *Radio Shack dictionary of electronics.*
48. R.H. Dyck, "Intensified CCD Camera Uses Fiber-Optic Coupling ," *Electronic Imaging*, May 1984.
49. Davis and Hau-Kuang Liu, "Optical-data-processing properties of a liquid-crystal television spatial light modulator," *Optics Letters*, p. 635, December 1985.

Vitae

The author was born on April 22, 1954 in State College, Pennsylvania. Before the author went to Reed College in 1972, he had moved eight times and attended ten different schools, including ones in Manhattan, Amsterdam, and Houston. He received a bachelors degree in Physics from Reed in 1977, and a Masters of Arts in Science Teaching in 1980. That same year he began studying at OGC.